UNIVERSITY OF CALIFORNIA SAN DIEGO

# Nutrient compositions in southeast Greenland waters and polar water influence on distribution

A Thesis submitted in partial satisfaction of the requirements
for the degree Master of Science

in

Oceanography

by

Matthew M. Brigham

Committee in charge:

Professor Fiammetta Straneo, Chair
Professor John Hildebrand
Professor Maria Vernet

2023

The Thesis of Matthew M. Brigham is approved, and it is acceptable in quality and form for publication on microfilm and electronically.

University of California San Diego

2023

TABLE OF CONTENTS

LIST OF FIGURES

LIST OF TABLES

## LIST OF ABBREVIATIONS

| | |
|---|---|
| AMOC | Atlantic Meridional Overturning Circulation |
| AW | Atlantic Water |
| BODC | British Oceanographic Data Centre |
| °C | Degrees Celsius |
| CCHDO | CLIVAR and Carbon Hydrographic Data Office |
| CTD | Conductivity, Temperature, and Depth |
| EGCC | East Greenland Coastal Current |
| EGC | East Greenland Current |
| IC | Irminger Current |
| IrSPMW | Irminger Subpolar Mode Water |
| ISOW | Iceland-Scotland Overflow Water |
| kg | Kilograms |
| km | Kilometers |
| LSW | Labrador Sea Water |
| m | Meters |
| mSv | milliSverdrup |
| μ | micro ($1 \times 10^{-6}$) |
| NAC | North Atlantic Current |
| ppt | Parts per thousand |
| POLW | Polar Water |
| PW | Pacific Water |
| PFW | Pacific Freshwater |

| | |
|---|---|
| PSW | Polar Surface Water |
| PSWw | Warm Polar Surface Water |
| SEANOE | SEA scieNtific Open data Edition |
| Sv | Sverdrup |

ACKNOWLEDGEMENTS

First, to my family – Mom, Dad, Caroline, and Zach, and to my fiancée, Gaby – thank you all for your support these past two years and always. I really appreciate all you do for me and the love you share.

To my advisor, Fiamma, who guided me throughout my research and helped me by recommending a thesis topic that aligned with my personal interests, providing assistance when needed. Thank you for your support in this process and for the opportunity to conduct research at Scripps.

To Jamie, thank you for your help throughout "my coding journey," as you always showed me the utmost patience and guided me throughout my research, particularly when I had no prior coding background.

To those on the OSNAP cruise and/or in the Ice/Ocean group – Aaron, Aurora, Bobby, Donald, Margaret, Monica, and Nicole. Thank you all for your help, support, and friendship. To those on the list that helped me with coding, thank you for your patience and instruction. Your teachings created the backbone for my coding knowledge and I have a lot to be thankful for in this group. I cannot thank you enough.

Finally, to Maria, thank you for your guidance and assistance with my analysis. Your instruction on biological oceanography really helped me to understand what was likely occurring biologically.

ABSTRACT OF THE THESIS

Nutrient compositions in southeast Greenland waters and polar water influence on distribution

by

Matthew M. Brigham

Master of Science in Oceanography

University of California San Diego, 2023

Professor Fiammetta Straneo, Chair

The convergence of freshwater from polar and subpolar waters influences nutrient (nitrate, phosphate, and silicate) concentrations on the southeastern Greenland shelf. Interannual variability of nutrient distributions from the shoreline to 150 km offshore were determined by using hydrographic and nutrient measurements from June to September of 2002 to 2016 to produce high-resolution transects. Although no significant trend was observed during the period analyzed, in-situ observations from 1991 to 2018 revealed considerable interannual variability and that nutrient concentrations in polar-origin waters (POLW) were two to three times less than those of Atlantic-origin (AW). In POLW, the mean

nitrate, phosphate, and silicate concentrations (in μmol/kg) were 5.02, 0.51, and 3.10, respectively, compared to that of AW, with means of 15.16, 0.98, and 7.80, respectively over the same area. Waters of Pacific-origin, transported through the Arctic Ocean circulation and western Fram Strait, were observed furthest inshore in southeastern Greenland from 1997 to 2018 with increased fractions of Pacific Water concentration in 2004 (0.15) and 2018 (0.16). From relationships observed between nutrients, nitrate was identified as the least biologically-available nutrient, followed by phosphate, and then, silicate, which concurred with previous studies in the North Atlantic region. The accepted global stochiometric relationships for N:P, N:Si, and Si:P are 16, 1.07, and 15, respectively. As expected, results differed slightly throughout the cross section, as the area from the shoreline to 72 km exhibited ratios of 17.71, 1.66, and 9.70, respectively, while the area from 72 km to 150 displayed ratios of 13.56, 1.00, and 10.14, respectively.

# CHAPTER 1: INTRODUCTION

## 1.1 Objectives and Background

The intention of this study was to analyze the mean and interannual variability in nutrient concentrations of nitrate ($NO_3^-$), phosphate ($PO_4^{3-}$), and silicic acid (referred henceforth as silicate: $Si(OH)_4$) in southeast Greenland waters within 150 km from the coast. Figure 1 below illustrates the study area. Nutrients in the water column along the southeast Greenland continental shelf and slope are largely linked to the transport of waters from the north Atlantic Ocean and Arctic Ocean, and the water masses that are present as a result. Increased freshwater discharge due to the rapid melting of the Greenland ice sheet and sea-ice in the Arctic Ocean are likely to impact the nutrient distribution in southeastern Greenland, as this additional freshwater flux influences circulation and stratification of these water masses. In this study, we first examined the mean distribution of nutrients on the shelf and slope and then, assessed the interannual variability in terms of changes in nutrient concentrations within the different water masses. This study will set the baseline for future studies of water mass and nutrient distribution variabilities, relative to marine ecosystems, along the southeastern Greenland shelf.

In this study, historical in-situ observations from 1991 to 2018, collected during the months of June to September, were used to investigate nutrient concentrations in different water masses and identify the source waters for the region of study. The time frame was chosen based on the availability of in-situ observations. All data sets used are identified and discussed in Chapter 2. The objectives of this study were to:

1) Describe the mean nutrient distribution on the southeast Greenland continental shelf and define interannual variability in nutrient observations.

2) Determine how nutrient concentrations differ between prominent Atlantic Ocean and Arctic Ocean water masses, and compare the mean and variability to previous studies.
3) Quantify the interannual variability in mean fractions of Pacific Water (PW) and Pacific Fresh Water (PFW) for samples in the Polar Water (POLW) water mass within the region of study.
4) Identify the relationships between nutrients and determine the bioavailability of these nutrients in relation to one another.

Part of this study was inspired by the results of Tuerena et al. (2021) that analyzed waters northeast of Greenland to calculate the mean nutrient concentrations of polar-origin water masses, similar to those analyzed in this study. Another part of this study was inspired by the work of Sutherland et al. (2009) who assessed the freshwater composition of waters off southeastern Greenland to identify the appropriate proportions of Pacific source water.

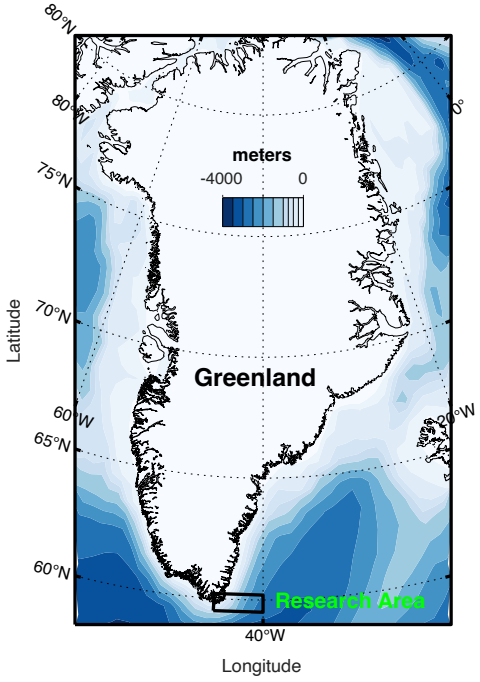


**Figure 1:** Research area indicated by the black box near the southern tip of Greenland. Bathymetric contours from 4000 m to surface are shaded from dark blue to white and are labeled as such.

The extensive subpolar North Atlantic (SPNA), spanning from 47ºN - 65ºN and 0ºW - 60ºW (Holliday et al., 2020), is an area potentially subject to large-scale freshening due to the mass loss of the Greenland ice sheet [GrIS] (Dukhovskoy et al., 2019; Rignot et al, 2008) and an accelerated loss of Arctic Ocean sea ice (Comiso et al., 2008). For instance, the mean annual freshwater export through western Fram Strait was variable between the 1990s to 2000s (Dickson et al., 2007; de Steur et al., 2009), but increased by 150% to 131 mSv in 2011 (de Steur et al., 2017). This freshening, coupled with an additional increase of GrIS runoff from 65 mSv in the early 1990s to 120 mSv in 2009 (Bamber et al., 2012) reveals a trend of wide-scale freshening. Freshwater transport influences marine ecology through increased nutrient availability (Tesdal et al., 2022), fostering biological productivity (Hopwood et al., 2018). For example, the GrIS, which covers around 80% of Greenland's total land mass (Vernet et al., 2021), has been noted as a significant source of nutrients including phosphorus (Hawkings et al., 2016), nitrate (Beaton et al., 2017), and silica (Meire et al, 2016) to marine environments fed by both marine and land-terminating glacial runoff. Nutrient flux also results from the buoyancy-driven upwelling of nutrient-rich waters at the base of glaciers, further contributing to biological productivity (Cape et al., 2019; Hopwood et al., 2018). With recent wide-scale freshening, understanding how nutrient concentrations will be affected by continued changes to stratification and circulation of waters on the southeastern Greenland shelf and slope is a topic of great importance. A study with these objectives in this area is the first of its kind amongst the scientific community.

### 1.2 Biological Productivity Trends and Factors

Factors influencing biological productivity along the Greenland coasts, continental shelf, slope and further offshore are numerous. Namely, the difference in air and seawater temperatures, Arctic sea ice flux through Fram Strait, upwelling of nutrient-rich waters, daylength, and angle of the sun all contribute to the maintenance of biological productivity in the region (Vernet et al., 2021; Hopwood et al., 2018). Each influence has a specific benefit to productivity.

Due to the large latitudinal extent of Greenland (59º46'N - 83º40' N) and the different oceanographic influences throughout, biological productivity results are skewed both in the measure of total net primary productivity and phytoplankton bloom initiation (Vernet et al., 2021). In a study conducted using two numerical models and data from 2008 to 2017 by Vernet et al. (2021), net primary productivity decreased by a factor of three to four times along Greenland shelves from south (~ 80 grams of Carbon per meters$^2$ per year [g C m$^{-2}$ yr$^{-1}$]) to north (minimum of 25 g C m$^{-2}$ yr$^{-1}$). Differences in net primary productivity also exist locally between the shelf area of southeastern Greenland and deeper waters off the shelf closer to the Irminger Sea, as inshore of the shelf yields a value of 40 g C m$^{-2}$ yr$^{-1}$ compared to ~ 80-100 g C m$^{-2}$ yr$^{-1}$ further offshore (Vernet et al., 2021). This extreme difference indicates that the presence of Atlantic water and upwelling of nutrients along the Deep Western Boundary Current just offshore of the eastern Greenland continental slope positively influences productivity in the region. Similar to net primary productivity, phytoplankton bloom initiation also experiences a south-to-north latitudinal gradient along Greenland. On average, in the waters of southwestern and southeastern Greenland, spring bloom initiation occurs a month to two months prior to blooms in the waters of central and northern Greenland, starting in mid-April and lasting for

approximately 3 weeks (Vernet et al., 2021). Within this study, the earliest measurements are taken in mid-June, well after this spring bloom regularly occurs, so these measurements are likely not linked to bloom dynamics. Instead, the circulation of currents and water masses in the North Atlantic and Greenland shelf are most representative of summer conditions, likely linked to interannual variations seen in this study and are discussed further below.

### 1.3 North Atlantic Circulation

The circulation regime in the North Atlantic subpolar gyre governs the rate at which deep water masses form (Katsman et al., 2004), which plays an integral role in the global sinking of anthropogenic carbon dioxide and in turn, global climate. As an introduction to the importance of research in this area, due to the presence of the Atlantic Meridional Overturning Circulation (AMOC) and ventilation of both North Atlantic Deep Water and LSW that occurs in the North Atlantic, this area stores approximately 23% of all oceanic anthropogenic carbon dioxide, which is the highest global percentage relative to the size of the area (Sabine et al., 2004). Understanding this region's circulation lays the framework for the comprehension of nutrient transport on the southeast Greenland shelf and slope.

The AMOC is primarily driven by the cooling of upper-ocean warm saline waters transported via the NAC in the northeastern Atlantic and Nordic Seas (Sarafanov et al., 2012). Formed by the northward-flowing warm waters of the Gulf Stream and the southward-flowing cold waters of the Labrador Current offshore of the Tail of the Grand Banks, the NAC crosses the North Atlantic from west to east and enters into the eastern basin (Buckley and Marshall, 2015). From here, the NAC branches. Described by Sarafanov et al. (2012), about 40% of this flow continues northeast towards the Nordic Seas where it is cooled, subducted due to an increase in density, and circulated equatorward at depth as ISOW (Buckley and Marshall, 2015);

thereby, forming the lower limb of the AMOC. This water continues southwest at depth, is bathymetrically forced around the Reykjanes Ridge at the Charles-Gibbs Fracture Zone, flows northerly to join with the IC and eventually, the Deep Western Boundary Current on the coast of southeastern Greenland (Sarafanov et al., 2012). The remaining 60% constitutes the AMOC's upper limb that circulates in the upper-ocean to the west, either meandering slightly around or crossing directly over the Reykjanes Ridge at the surface and mid-depths, and joining with the IC to circulate cyclonically around the Irminger Sea (Sarafanov et al., 2012). Both the upper and lower limbs' action of the AMOC support the necessary heat transport from the south and freshwater transport from the north. Once waters have circulated to southeastern Greenland, all currents at all depths in the region eventually round the southern tip of Greenland at Cape Farewell and continue northwest along the coast of southwestern Greenland and west towards the Labrador Sea, further transporting freshwater (Buckley and Marshall, 2015).

### 1.4 Southeast Greenland Shelf Circulation

Within this study's research area and from the mid-1990s to 2010, southeast Greenland was noted as the Greenland ice sheet region with the largest freshwater flux (Bamber et al., 2012). Given this highly active area of glacial melting due to increasing temperatures and because very little freshwater is lost offshore (Dickson et al, 2007) as waters are transported via currents south along the coast, these currents play a key role in the transport of nutrients south and towards the open ocean. For instance, in southeast Greenland, it is estimated that as much as 60% of all meltwater runoff in the area is transported south and west into the northern Labrador Sea (Luo et al., 2016). These currents are critical to the continuity of nutrient fluxes and transport along southeastern Greenland. Increased freshening of near-surface waters may have an effect on these currents in the future.

Within the region and throughout the southeastern side of Greenland, there exists three prominent nearshore currents: the EGC, EGCC, and IC (mentioned in the previous section). Waters with low salinity exit the Arctic Ocean through the western side of Fram Strait, an area northeast of Greenland, via the EGC (Sutherland et al. 2009). Further south, in an area below the Denmark Strait, part of the EGC bifurcates into the much smaller, 20 km-wide EGCC, which occurs closer to the shoreline. Discovery and studies of the EGCC are fairly recent, so it is believed that this bifurcation occurs due to bathymetric steering, but it could also be caused by stratification and ambient flow strength (Sutherland and Pickart, 2008). The EGC and EGCC have mean volume transports of 18 ± 1 Sv and 0.86 ± 0.1 Sv, respectively, while the mean freshwater transports for both currents is 32 ± 6 mSv and 42 ± 6 mSv, respectively (Le Bras et al., 2018). For reference, 1 Sv is equal to 1 x $10^6$ $m^3$/second. With a combined transport of approximately 2 Sv when measured from 68ºN to Cape Farewell and freshwater transport of 38 ± 9.9 mSv from Denmark Strait to Cape Farewell, the EGCC/EGC system is a prominent force for freshwater transport along the eastern side of Greenland (Sutherland and Pickart, 2008). Slightly offshore of the EGC exists the IC, a southerly current that transports waters with high salinity of Atlantic origin that have cyclonically circulated within the Irminger Sea. Given the proximity of the IC to the EGC, the IC also transports freshwater of Arctic origin along the coast of southeast Greenland. Together, the EGC, EGCC, and IC account for approximately 70% of the total freshwater transport, with maximum transports occurring in late fall and winter (Le Bras et al., 2018).

### 1.5 Source waters and Arctic Ocean water masses

In the region of study, there are two main source waters from the Pacific (PW) and Atlantic (AW) Oceans, the latter of which was partially discussed in section 1.2 of this study.

PW flows north through the Bering Strait, passes through the Chukchi Sea, and proceeds to the Canada Basin north of Canada. Some of these waters meander between the islands of the Canadian Arctic Archipelago, exiting the Arctic Ocean, while others continue circulating (Dodd et al., 2012). Other waters do not immediately exit, as their average residence time in the Arctic ranges from five to eleven years, depending on research sources (Sutherland et al., 2009). Once in the Arctic basin, these waters mix with AW that has entered through the eastern side of Fram Strait (the only Arctic pathway with two-way exchange of inflow and outflow waters) and both the Barents and Kara Seas (Rudels et al., 2015; Dodd et al., 2012). During circulation in this basin, additional sources of freshwater are introduced including sea ice melt, glacial ice meltwater, direct precipitation, and river water via runoff (Dodd et al., 2012). With these contributions to the Arctic in mind, there exists two primary water masses that are applicable to this study: PSW and PSWw. PSW is identified as waters with a potential density of less than or equal to 1027.7 $kg/m^3$ and a potential temperature of less than or equal to 0°C, while PSWw has the same potential density range or is lighter than PSW and a potential temperature that is greater than 0°C (Rudels et al., 2005, Sutherland and Pickart, 2008). PSW is the cold and low saline surface waters that act as a boundary between the sea ice and AW below, and PSWw is PSW that has been warmed due to intrusions of AW, solar heating, and other air-sea interactions (Rudels et al., 2005; Jones et al., 2021). Both characteristics of PSW and PSWw were considered to identify nutrient concentrations in the polar water mass discussed later in this study. Following residence in the Arctic Ocean and if not exported via the Canadian Arctic Archipelago, waters exit through the western Fram Strait and contribute to the EGC, discussed in the previous section.

Given the oceanographic pathways that both source waters take to reach southeastern Greenland, each contains water that differs in several properties. Waters originating in the

Atlantic Ocean are characterized by nutrient-rich waters associated with water mass formation and transport. For waters originating in the Pacific Ocean, this water's nutrient contents have been altered from source water concentrations. When PW flows over the Chukchi Sea, this transit modifies the seawater by processes of mixing with runoff, production and decay of organic matter (Jones et al., 1998), atmospheric deposition, and biological processes. These biological processes include denitrification, in which nitrate is used by nitrogen-fixing organisms to oxidize organic material, releasing nitrogen gas into the atmosphere and depleting nitrate relative to phosphate in the water column (Yamamoto-Kawai et al., 2006; Jones et al., 2003). The shelves of both the Bering and Chukchi Seas are sites where denitrification occurs, where water was calculated to have about 0.8 μmol/kg of excess phosphate compared to nitrate after exiting this area and continuing east towards the Beaufort Sea (Yamamoto-Kawai et al., 2006). Another biological process that may occur in these waters where nitrate is depleted but phosphate is not is nitrogen fixation, where an increase in this process would lead to less PW in the sample (Jones et al., 2003). The fractions of PW and PFW contained within a sample can be calculated using the known relationship between concentrations of nitrate and phosphate for PW source waters (Jones et al., 2008a). These calculations were completed and methods for doing so are discussed more in section 2.2.4.

This study is the first of its kind, as no previous research has analyzed the interannual variability of PW and PFW fractions over this time scale within this study area. A motivation for quantifying this variability is to understand the flux of freshwater exiting through Fram Strait and identify what remnants of PW exist in southeastern Greenland over time. Although other fractions of freshwater including meteoric water and sea ice melt were not explicitly calculated in this study due to the availability of data, a low fraction of PFW would indicate that the

majority of seawater collected from each measured sample is primarily composed of other freshwater sources, like those mentioned previously.

### 1.6 Importance of Biogeochemical Tracers and the Redfield Ratio

Biogeochemical tracers, also known as inorganic nutrients (e.g. nitrate, phosphate, and silicate), are vital to the sustainment of marine photosynthesis and overall marine ecosystem health. Prior to entering the ocean, elements of nitrogen, phosphorus, and silica undergo processes that ionize each element into inorganic nutrients. These nutrients are gradually cycled from various sources to the ocean and utilized in several processes (namely, growth and photosynthesis). Once used by marine microorganisms or if not utilized, these nutrients sink through the water column and are sluggishly cycled through the world's oceans. Studies show that it may take a few hundred years before dissolved phosphorus or silica reaches great depths and is upwelled to the photic zone; however, if these dissolved elements become mixed with marine sediments on the ocean floor, piled in layers, this process may take millions of years before inorganic ions containing these elements re-emerge via underwater volcanoes (Garrison 2010). On average, nitrate, phosphate, and silicate have average residence times in the ocean of five thousand years, fifty thousand years, and eight thousand years, respectively (Toggweiler 1999; Moore et al., 2013; Tréguer and De La Rocha, 2013). Each of the three inorganic nutrients studied here are introduced into the marine ecosystem through different pathways, utilized in different ways, and exported differently.

Just as these inorganic nutrients are transported via different methods, the elements that are incorporated are found in different quantities within the marine environment. A fundamental principle of ocean biogeochemistry is that the elements of Carbon (C), Silica (Si), Nitrogen (N), and Phosphorus (P) exist in marine planktonic species and throughout the water column as a

ratio. This Redfield ratio was originally defined in terms of C:N:P as 106:16:1 by assessing global surface plankton nutrient uptake requirements and hypothesizing that at-depth nutrients were associated with sinking and rimineralized plankton (Redfield 1958). This ratio was later redefined to include Silica as a ratio (C:Si:N:P) of 106:15:16:1 and named the Redfield-Brzezinski ratio (Brzezinski 2004). As dissolved ions containing the above elements are assimilated at the surface and released via respiration at depth, this ratio can be applied to the dissolved inorganic nutrients assessed in this study. It is important to note that the Redfield ratio is not consistent throughout all marine environments, as elemental stoichiometry displays a latitudinal gradient and also differs based on plankton community composition. For instance, research indicates that in-situ ratios tend to be higher (177-195:22-28:1) than the accepted Redfield ratio in gyres with fewer nutrients and more oxygen at depth that are deemed oligotrophic, similar (109-137:16-18:1) to the Redfield ratio in upwelling regions, and less than the Redfield ratio (63-78:13:1) where an abundance of nutrients is present in polar environments (Martiny et al., 2013a and 2013b; Quay 2021; and Teng et al., 2014). Similarly, differences in plankton community biodiversity also skew in-situ ratios, as different taxonomic plankton lineages consume nutrients at different rates (Quigg et al., 2003; Moore et al., 2013; Paytan and McLaughlin, 2007). Even though the canonical Redfield ratio differs from in-situ observations based on a variety of factors, it remains justifiable to compare this ratio to measurements in this study, as these comparisons are universal across literature.

### 1.6.1 Nitrate

Just as each inorganic nutrient is found at different quantities throughout the world's oceans, their sources to the marine environment are equally unique. Nitrate is supplied via several pathways including terrestrially in runoff from soil (Garrison 2010), from depth through

upwelling of nitrate-rich deep water (Zehr and Ward, 2002) and convective overturning (Voss et al., 2013), and transported from the atmosphere. In the Nitrogen cycle, dinitrogen gas from the atmosphere dissolves at the ocean's surface through a process called nitrogen fixation and is fixed by diazotrophic cyanobacteria (blue-green algae) mostly of the genus *Trichodesmium* (Bergman et al., 2013; Capone et al., 1997) into biologically-available inorganic nitrogen in the form of ammonium or ammonia (Lalli and Parsons, 1993). This process is globally ubiquitous, occurring on the magnitude of ~80 Teragrams (Tg) of Nitrogen (N) fixed by *Trichodesmium* annually (Capone et al., 1997), which is a significant portion of the global nitrogen fixation range of 100-200 Tg N per year (Karl et al., 2002). These inorganic forms of nitrogen within the water column are oxidized by eukaryotic species including foraminifera (Voss et al., 2013) to nitrite and then, nitrate in a two-step progression called nitrification (Lalli and Parsons, 1993), which occurs primarily in the lower portion of the euphotic zone (Zehr and Ward, 2002). Once it is made biologically-available, nitrate is used by several marine microorganisms.

Nitrate is consumed by all photosynthetic eukaryotes, including the phyla Chlorophyta (green algae) and Rhodophyta (red algae), through processes of nitrate assimilation where nitrate enters the cell, is catalyzed by an enzyme called nitrate reductase into nitrite and transported to the chloroplast, where the nitrite reductase enzyme reduces it further to ammonium (Sanz-Luque et al., 2015). However, nitrate assimilation is not restricted to eukaryotes, as some species of prokaryotic cyanobacteria, namely genera *Synechococcus* and *Prochlorococcus*, contain assimilatory nitrate reductase genes and can also conduct this process (Zehr and Ward, 2002). Furthermore, ammonium is catalyzed into several amino acids, namely glutamine via an enzyme called glutamine synthetase (Sanz-Luque et al., 2015). These amino acids are used in protein synthesis, which are vital for growth of phytoplankton. Finally, if nitrate remains unused and

sinks through the water column, it is known that between 20-78% is transported by large oceanic diatoms such as *Rhizosolenia* that migrate to nutrient-rich deep water below 100 m to obtain other nutrients, returning to the surface later and carrying nitrate (Villareal et al., 1999). The incorporation of nitrate into the marine environment is critical to the growth and sustainment of phytoplankton.

Due to low residence times when compared to other nutrients in this study, nitrate is not identified as the most limiting nutrient globally, but still remains in short supply relative to its demand and often limits growth because of this. 'Liebig's law' states that growth is not determined by the combined nutrients available, but is instead, limited by the scantest nutrient (Tyrrell 1999). If one nutrient that was previously limiting becomes more available than another, the next scarcest nutrient becomes the nutrient that limits growth in the ecosystem. It is possible to have two co-limiting nutrients at once, where the addition of either would significantly contribute to growth (Warsi and Dykhuizen, 2017). In the North Atlantic nearby the region of this study, the limiting nutrient is nitrate, followed closely behind by phosphate, and then, silicate (Moore et al., 2013).

### 1.6.2 Phosphate

Due to its long residence time and because it is unable to be fixed from the atmosphere, phosphate is identified as the limiting nutrient in marine ecosystems over long geologic time scales (Paytan and McLaughlin, 2007). Similar to nitrate, the presence of phosphate is essential to marine photosynthesis and growth.

Phosphate is primarily introduced into oceanic environments through continental weathering (Paytan and McLaughlin, 2007) and delivered via riverine flux (Tyrrell 1999). Introduction of phosphate from mineral dust (particularly offshore), aerosols, and volcanic ash

via atmospheric deposition also exists at trace quantities (Benitez-Nelson 2000). Anthropogenic sources of phosphate from terrestrial plant fertilizers are also plentiful with an estimated doubling of natural flux caused by erosion, sewage, and other human-origin means (Paytan and McLaughlin, 2007). Once introduced into the marine ecosystem, phosphate is a key component to several processes needed for photosynthesis and growth of marine microorganisms. During photosynthesis and in a process called photophosphorylation, phosphate is absorbed and brought to the thylakoid membrane of the chloroplast, where an enzyme called adenosine triphosphate (ATP) synthase generates ATP (provides energy for all cellular processes) using adenosine diphosphate (ADP) and the absorbed phosphate ion (Demirel and Gerbaud, 2019; Yahia et al., 2019). Finally, phosphate is also used in nucleic acids, which form the genetic material (deoxyribonucleic acid [DNA] and ribonucleic acid [RNA]) of all organisms, and phospholipids, allowing the cells of photosynthetic organisms to be selective in absorption by forming semi-permeable membranes (Lordan et al., 2017; Biology Dictionary, 2017). Phosphate is a key ingredient needed for successful and continued photosynthesis of marine microorganisms.

### 1.6.3 Silicate

As the least limiting nutrient in the North Atlantic compared to others in this study, silicate in the marine environment is in adequate concentrations to the microorganisms that use it for growth. Silicate is similar to phosphate in that it is predominantly sourced through continental weathering and transported by riverine flux, as over 70% of all oceanic dissolved silica comes from this input (Hawkings et al., 2017). Additional sources of silicate include submarine groundwater discharge, aeolian dust deposition, high-temperature hydrothermal vents, low-temperature dissolution of oceanic seafloor basalts, and weathering of both glaciers and ice sheets (Tréguer and De La Rocha, 2013; Hawkings et al., 2017). In this study's region and

throughout Greenland, it is estimated that the Greenland ice sheet delivers a total Si flux of up to 0.79 Terramoles per year, which equates to approximately 8% of the global flux to the ocean (Hawkings et al., 2017), a staggering figure when considering the size of Greenland in relation to all global land mass. Once biologically available, silicate is used for biomineralization of shells in several microorganisms. In marine phytoplankton species of diatoms and silicoflagellates (golden-brown algae), these structures are called frustules and spicules, respectively (Lalli and Parsons, 1993). Typically, a majority of algae species construct their cell walls from organic material (i.e. cyanobacteria) or calcium carbonate (i.e. dinoflagellates, foraminifera, and coccolithophorids), so these silicate structures are in contrast to most others (Durak et al., 2016). Of those microorganisms that utilize silicate for growth, diatoms are of extreme importance. Contributing up to 45% of all marine primary production (Tréguer et al., 1995) and around 20% of all photosynthesis on Earth (Armbrust 2009), the role that diatoms play cannot be understated. When these microorganisms die or are eaten and excreted, silicate can take several paths. It either sinks slowly through the water column and is dissolved at depth to be recycled later or collects in the benthic environment as several layers of globigerina ooze, remaining as such for longer time scales (Dipper 2022). Within this ooze, silicate is dissolved further into biogenic silica, which is later upwelled and remineralized again by diatoms and other silica-requiring organisms closer to the surface. Required by some of the most prolific microorganisms for growth, silicate is essential to continued primary productivity in the world's oceans.

### 1.7 Nutrient Cycling in the region

The cycling of nutrients via deep water convective overturning and surface current circulation aids in the sustainment of the marine ecosystem in the North Atlantic. Previous studies have conducted observations in the broader region, which have generally indicated a

decrease of nutrients closer to the surface (mostly due to cellular respiration and photosynthesis) and an increase at depth with higher concentrations existing in the benthos (i.e. García-Ibáñez et al., 2015). Nutrient concentrations have also been linked to water masses in the broad North Atlantic region that have primarily reviewed open-ocean water masses (Johnson et al., 2013, García-Ibáñez et al., 2015). For example, in this region beyond the Greenland shelf and slope at depth exists Denmark Strait Overflow Water, which has mean nitrate, phosphate, and silicate concentrations of 14.1, 1.1, and 7.8 μmol/kg, respectively (García-Ibáñez et al., 2015). However, limited research on this topic has been conducted on waters closest to Greenland, particularly along the shelf and slope. No previous study has assessed shelf cross sections of nutrients and questioned interannual variability nor investigated nutrient concentrations in water masses within this specific region. This study aims to examine these trends and report on all findings associated with nutrients in southeastern Greenland.

# CHAPTER 2: DATA AND METHODS

## 2.1 Data

### 2.1.1 Biogeochemical Tracers and CTD: Sampling

Beginning in the early 1970s and up to current day, in-situ observations made by research vessels and various watercraft have been the primary means to monitor nutrient concentration and water properties within the seawater column throughout the world's oceans. This data is publicly available online via numerous databases. Where sea ice conditions permit safe passage to these vessels, this data provides a record of observations utilized by scientists and research parties from around the globe.

When sampling for biogeochemical tracers, procedures vary between cruises. Generally, seawater samples are collected using a multi-bottle rosette equipped with equal-sized Niskin sampling bottles. After a bottle has reached a depth that is identified as suitable for collection, the operator on the vessel sends a trigger down the cable connected to the rosette that signals the bottle to close. Once closed, the bottle is sealed at both ends, prohibiting seawater intrusion from other depths as the rosette is raised from depth. Sampling of seawater ends after the appropriate bottles have been released and the rosette has been brought to the surface. Once onboard the vessel, for nutrient sampling, scientists extract water samples from the bottles using a dark container that restricts light penetration that may alter calculated concentration values. Samples are either analyzed onboard using a segmented flow analyzer (e.g. SOC Chemlab AAII type Auto Analyser, etc.) or similar method within twenty-four hours of collection (García-Ibáñez et al., 2015). If not sampled onboard, seawater samples are filtered and placed into a dark container before being stored at below freezing temperatures and analyzed at a later date. To measure CTD, an instrument (e.g. Neil Brown Mark III, Seabird 911+, etc.) is attached to the rosette and

operates autonomously throughout the lowering and raising of the rosette (García-Ibáñez et al., 2015). Inputs from this instrument are used by the computer to determine salinity and temperature at given depths. Frequently, water samples collected via Niskin bottles are utilized to measure salinity at given depths via a salinometer, which are cross-referenced to CTD readings, calibrating the instrument. Other methods are used to ensure calibration of measurements onboard.

Prior to submittal for database retention, CTD measurements and nutrient concentrations are corrected for accuracy via various methods. For instance, for datasets listed in Table 1 as 1997d, 1997e, 2002b, 2004, 2006, 2008a, and 2010a within Section 2.1.3 of this study, CTD measurements were adjusted for accuracy to 1 decibar for pressure, 0.002 °C for temperature, and 0.003 ppt for salinity, while bottle measurements were evaluated at 0.2, 0.02, and 0.1µmol/kg for nitrate, phosphate, and silicate, respectively (García-Ibáñez et al., 2015). All datasets encountered some form of data accuracy and calibration prior to being logged into online databases. These calibration techniques and associated procedures are located within each cruise's cruise report often found at the website locations listed in References, as available.

### 2.1.2 Data Extraction and Processing

Within databases, data is found in various formats and types of files (e.g. .txt, .nc, .csv, .mat, etc.) and distinguished by latitude, longitude, and time. In determining the area of study, oceanographic characteristics of currents and water masses were considered. As limited previous research has been conducted on interannual nutrient variability in the area and given the southeast Greenland shelf is a region of high biological productivity, this research area was chosen for analysis. A box with coordinate dimensions of latitude range 59.5°N to 65°N and longitude range of 35°W to 44°W box was determined and datasets were extracted based on

these parameters. In identifying that the southernmost area of the box had the most consistently available data between years, the box was further limited to coordinate dimensions of latitude range 59.5°N to 60°N and longitude range of 35°W to 44°W. Additionally, it was noted that the majority of data was collected during summer months, so data compilation was further restricted to the months of June to September for assessment of interannual variability in summer trends, as these months' data was most prevalent. When available, CTD data was also compiled to examine trends, but was only utilized when nutrient data had minimum separation between casts. When not available, temperature and salinity data samples that were collected with nutrient bottle samples were gathered and used in analysis. The usage of CTD data versus salinity and temperature data collected via nutrient sampling is annotated appropriately throughout this study.

At the start of data allocation, all data obtained was from 1981 to 2018. After noting that the only dataset that spanned the 1980's was from 1981, and to avoid a large time gap between 1981 and the next chronological dataset in 1991, the data from 1981 was excluded from analysis. For several datasets, data was separated by individual bottle and CTD files. In these cases, files for each dataset were combined appropriately for ease of data usage. Additionally, variables associated with time for several datasets were adjusted to be read as datetime within Matlab, rather than their respective given formats. Other variables were also adjusted as needed to ensure continuity of units and measurements (i.e. micromoles/liter converted to micromoles/kg, negative nutrient concentrations changed to zero). The thermodynamic equation of seawater was utilized to convert all in-situ temperature observations to potential or conservative temperature and salinity measurements to absolute salinity (The Gibbs Seawater (GSW) Oceanographic Toolbox of TEOS-10) for use in plotting potential density. Published literature sources also cite potential temperature for water mass defining characteristics used later in this analysis. Ensuring

all data was in the same format was essential to continuity of analysis for research purposes. For analysis within the region and time period identified, nineteen datasets were gathered and are listed in Table 1 found in Section 2.1.3.

Plotting the data in latitude and longitude coordinates led to the identification of five datasets (2010a, 2012, 2014, 2016a, and 2018) that had similar coordinates where nutrient data was collected and when plotted, formed two distinct and connected straight lines of hydrographic stations pointing southeasterly from the coastline to offshore. Utilizing the bathymetry profile from Matlab's m-map mapping package via Etopo2 (Pawlowicz 2020), a bathymetry profile was extracted and plotted, revealing that the second distinct line occurred just beyond the 1000 m isobath. This bathymetry profile was verified using the bottom depth values from each cast and dataset listed above, confirming that Etopo2's depth curve was suitable for use in analysis.

### 2.1.3 Data Gridding and Interpolation

Given one of the study's purposes was to describe biogeochemical trends on the continental shelf, interpolating the datasets onto a distance-depth grid aided in this evaluation. Similar to the analyses conducted by Våge et al. (2011) and Tesdal et al. (2022), a least squares regression line was fitted to each station's latitude and longitude of the two distinct lines of grouped stations, determining the point at which the inner regression line intersected the coastline. These two regression lines were plotted from the coastline to the pivot point at 71.7 km in the direction of the first grouping of stations and from the same pivot point to 150 km from the coastline in the direction of the second grouping, respectively. Each section of gridded points will henceforth be referred to as the "inner shelf" (coastline to pivot point) and "outer shelf" (pivot point to 150 km). Both sections were gridded at a vertical depth resolution of 10 m throughout the water column (301 total points by depth) and at 100 m resolution for the distance

from the Greenland coast (1501 total points at surface), forming a two-dimensional continuous grid from 0 km at the coastline to 150 km at the furthest gridded point and 0 m depth to 3000 m depth. These gridded points are illustrated as a grey continuous scatter plot in Figure 2 with the five datasets used to create the grid also labeled appropriately. It is noted that these datasets had stations that existed beyond the furthest 150 km gridded point. If further conditions for gridding listed below were not met, these station's data and other dataset's data exhibiting this distance from the gridded points were excluded from interpolation and analysis.

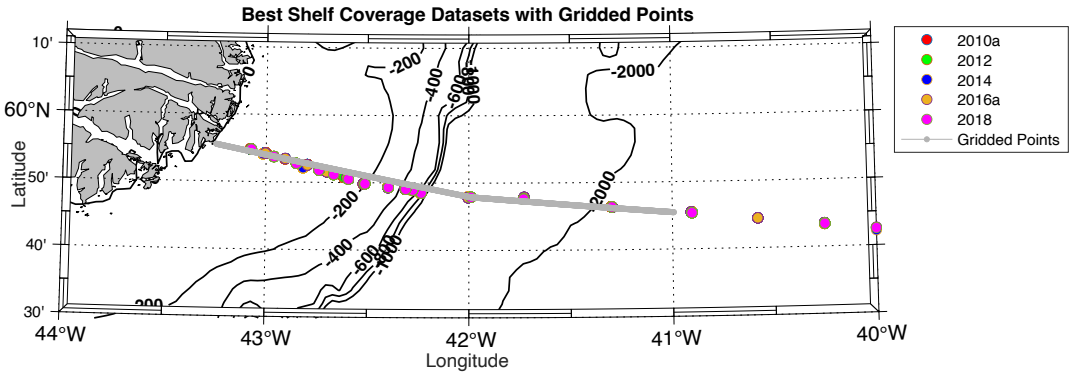


**Figure 2:** Datasets 2010a, 2012, 2014, 2016a, and 2018 are plotted in various colors, while gridded points for interpolation of all datasets is plotted in grey. The southeastern Greenland coastline is shaded grey. The 200, 400, 600, 800, 1000, 2000 m isobaths are shown in black and labeled as such.

For the purposes of gridding the data from all nineteen datasets, the distance between each hydrographic station and the closest gridded point was calculated. This distance was utilized to determine which casts to remove prior to interpolation, ensuring that gridded data in each dataset was represented appropriately in location along the grid. Given the inner shelf section covered rapidly changing bathymetry and with the presumption that nutrient and CTD data is likely more variable in the water column at different locations longitudinally at shallower depths along the coast, a 10 km maximum distance perpendicular to the gridded points was

determined for the inner shelf section. For stations occurring within the inner shelf area, those that were outside of 10 km from the closest gridded point were removed from interpolation. A final list of datasets with bottle data within the inner shelf section were 1997d, 2002b, 2004, 2005, 2006, 2007, 2008a, 2008b, 2010a, 2012, 2014, 2016a, and 2018. Conversely, for data located in the outer shelf area, this maximum limit was increased to 30 km to the closest gridded point with the belief that changes in both nutrient and CTD data are not as dynamic for station positions located further offshore and with more constant bathymetry. A final list of datasets with bottle data within the outer shelf section were 1991a, 1991c, 1997a, 1997e, 2002b, 2004, 2005, 2006, 2007, 2008a, 2008b, 2010a, 2012, 2014, 2015, 2016a, 2016b, and 2018. The complete list of all nineteen datasets with appropriate identifiers used in this analysis is listed in Table 1 below.

**Table 1:** Datasets utilized in analysis identified by cruise expedition code (expocode), year of data collection, letter identifier used in analysis, dates of data within analysis region and timeframe following interpolation, vessel that collected the data, and source of dataset via principal investigator(s) and database.

| Cruise Expedition Code | Years & Identifier | Dates | Vessel | Source |
|---|---|---|---|---|
| 06MT18_1 | 1991a | 5-6 Sep | R/V Meteor | Meincke (CCHDO) |
| N/A (RRS Charles Darwin Cruise 62) | 1991c | 16-17 Aug | RRS Charles Darwin | Gould (BODC) |
| 06MT39_4 | 1997a | 9 Aug | R/V Meteor | Schott (CCHDO) |
| 74DI230_1 | 1997d | 31 Aug | R/V Discovery | Bacon (CCHDO) |
| 06MT19970815 | 1997e | 25 Aug | R/V Meteor | Key (CCHDO) |
| 35TH20020610 | 2002b | 18 - 19 Jun | N/O Thalassa | Mercier (CCHDO) |
| 35TH20040604 | 2004 | 11 - 14 Jun | N/O Thalassa | Huck (CCHDO) |
| 64PE20050907 | 2005 | 17 Sep | R/V Pelagia | Veth (CCHDO) |
| 06MM20060523 | 2006 | 15 -16 Jun, 19 -22 Jun | R/V Maria S. Merian | Lherminier (CCHDO) |
| 64PE20070830 | 2007 | 12 - 13 Sep | R/V Pelagia | Brummer (CCHDO) |
| 35TH20080610 | 2008a | 2 - 3 Jul | N/O Thalassa | Mercier (CCHDO) |
| 74DI20080820 | 2008b | 6, 8 - 9 Sep | R/V Discovery | Bacon (CCHDO) |
| 35TH20100610 | 2010a | 29 - 30 Jun | N/O Thalassa | Huck and Mercier (CCHDO) |
| 29AH20120622 | 2012 | 16 - 17 Jul | R/V Sarmiento de Gamboa | Rios (CCHDO) |
| 35PK20140515 | 2014 | 15 - 17 Jun | R/V Pourquoi Pas? | Perez et al. (SEANOE) |
| 64PE40020150711 | 2015 | 23 - 24 Jul | R/V Pelagia | per comms. with M. de Jong and L. de Steur |
| 29AH20160617 | 2016a | 12 - 13 Jul | R/V Sarmiento de Gamboa | Perez (CCHDO) |
| N/A | 2016b | 7 - 19 Aug | R/V Neil Armstrong | per comms. with M. Cape for Pickart |
| 35HT20180611 | 2018 | 05 - 07 Jul | N/O Thalassa | Lherminier et al. (SEANOE) |

With data outside of these respective limits removed from both shelf sections, all datasets were interpolated onto the distance-depth grid and compared, plotting each nutrient concentration (nitrate, phosphate, and silicate) by depth. For those datasets that also had CTD data available, the same process was conducted for those stations, removing applicable CTD stations and interpolating the remaining stations onto the distance-depth grid. When creating these interpolated fields, some nutrient and CTD casts were removed, as including them created

an unnatural signal (i.e. significant increases or decreases in the variable being measured at similar depths and location within the grid that were obviously not present in the environment or isopycnals that sporadically changed by cast location). Following removal of all applicable casts, all nineteen dataset's casts included in analysis can be found in Figures 3 and 4 within the next section.

## 2.2 Methods

### 2.2.1 Nutrient Data Means

The process of calculating a mean plot for each nutrient variable, CTD potential temperature, and CTD salinity across the distance-depth grid and comparing this to each dataset allowed for more effective interannual trend analysis. Following interpolation of all datasets onto the gridded points, it was determined that only eight datasets had continuous nutrient station coverage of both inner and outer shelf sections. This was important to note because calculating a mean from interpolated data using datasets that do not have continuous interpolation from one cast to another would cause that mean to be skewed. For instance, data interpolation can only occur between two cast coordinate points. If one cast is a great distance from another cast (where the interpolation between them will not cover the entire water column, specifically in an area where bathymetry is changing rapidly), including these datasets into the mean would not allow for accurate depth coverage to be calculated, skewing the mean data. Therefore, the datasets with the most continuous coverage (2002b, 2004, 2006, 2008a, 2010a, 2012, 2014, and 2016a) were utilized to create an average for each nutrient, CTD potential temperature, and CTD salinity. Datasets not factored into the mean were not compared to the mean plots generated by the above eight datasets. Found below, Figures 3 and 4 illustrate the cast locations where nutrient data was collected following removal of casts outside of the respective thresholds (inner: 10 km, outer: 30

km from the gridded points) for the inner and outer shelf, respectively. Figure 3 details these locations for the datasets used in calculating the mean and Figure 4 details the remaining eleven datasets not listed above.

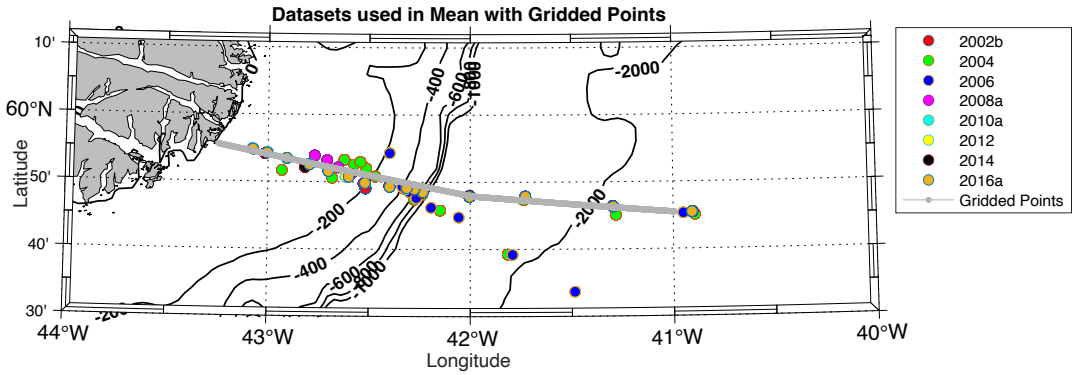


**Figure 3:** Cast locations for datasets used to calculate the mean plotted in various colors, while gridded points for interpolation of all datasets is plotted in grey. The southeastern Greenland coastline is shaded grey. The 200, 400, 600, 800, 1000, and 2000 m isobaths are shown in black and labeled as such.

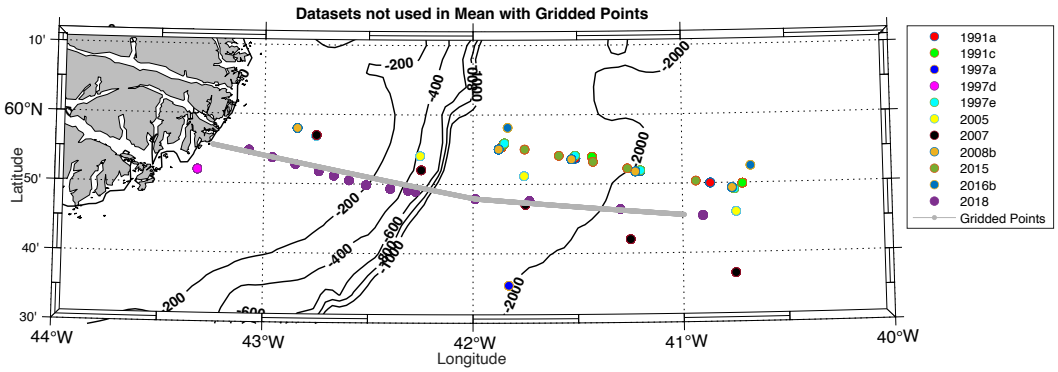


**Figure 4:** Cast locations for datasets not used to calculate the mean plotted in various colors, while gridded points for interpolation of all datasets is plotted in grey. The southeastern Greenland coastline is shaded grey. The 200, 400, 600, 800, 1000, and 2000 m isobaths are shown in black and labeled as such.

To calculate the mean, each of the eight datasets found in Figure 3 was added together across all interpolated distance-depth grid values and divided by the number of datasets, excluding values listed as “not a number” (NaN). After creation of the mean plots, it was clear that additional smoothing of the interpolation curves was required, as plotted nutrient and

potential density spatial distributions were unnatural. To further smooth the interpolations, the mean of each point in the distance-depth grid was further averaged twice in the distance space at an interval of 5 km on either side of the observation. For example, an interpolated value at depth 30 m and distance 100 km would be averaged with the interpolated values of congruent depth and interpolated values at distances between 95 km and 105 km. Then, this new average would be averaged again by repeating the first step of averaging the new mean with the new interpolated values at depth 30 m and new interpolated values between distances of 95 km and 105 km. For interpolated values with distance less than 5 km or greater than 145 km within the grid, these values were not capable of being averaged using distances that were outside of 0-150 km grid, so the values remained the same as the first averaging. The second-averaging of values with distances between 5 km to 145 km allowed for accurate representation of trends as they would appear in the field. Representation of these calculations is found in Equations (1), (2), and (3) below. Each of these datasets had all nutrient variables except for 2014, which contained no phosphate data. Therefore, 2014's dataset was not included in the mean of phosphate data.

$$M(d,z) = \frac{1}{n}\sum_{d=0}^{1501}\sum_{z=0}^{301} N(d,z) \qquad (1)$$

$$M_1(d,z) = \frac{1}{101}\sum_{d=51}^{1451}\sum_{z=0}^{301}(M(d,(z-50{:}\,z{:}\,z+50)) \qquad (2)$$

$$M_2(d,z) = \frac{1}{101}\sum_{d=51}^{1451}\sum_{z=0}^{301}(M_1(d,(z-50{:}\,z{:}\,z+50)) \qquad (3)$$

Above, $M$ is the mean nutrient, $M_1$ is the mean nutrient after the first averaging by all same depth observations from 5 km less and 5 km more within the grid, and $M_2$ is the mean nutrient after the second averaging in the distance space using the same method. Given this

process was repeated for all nutrients and additional variables, $M$, $M_1$, and $M_2$ also corresponds to calculations of mean CTD potential temperatures or salinities. In equation (1), $n$ is the number of datasets being averaged, $N$ is the nutrient, CTD potential temperature or salinity values of each dataset being summed as a function of distance ($d$) from 0 km to 150 km with spacing of 0.1 km (1501 total observations) and depth ($z$) from 0 m to 3000 m with spacing of 10 m (301 total observations) along the grid. In equations (2) and (3), the summations are divided by 101, as the total number of observations from 5 km less to 5 km more than the observation being averaged totals 101. The distance bounds of 51 (5 km) to 1451 (145 km) are representative of the averaging for all observations within that range. As mentioned previously, for observations that lie outside of the above range (i.e. less than 5 km and greater than 145 km distance), these interpolated values were not averaged and remained equivalent to the $M$ values from the first step when all datasets were averaged together.

After calculation of interpolated mean values for every variable at all appropriate depths and distances within the grid, differences between each dataset and the mean for that specific variable were calculated using equation (4) below.

$$\Delta = [M_2(d,z) - D(d,z)] \qquad (4)$$

In equation (4), the $\Delta$ symbol is representative of the difference between the final averaging minus the dataset's ($D$) original interpolated values for all values from d = 0 to 1501 and from z = 0 to 301, encompassing all interpolated values within the gridded section. The results for these means are found in Figures 5 through 9 within sections 3.1 and 3.2 of this study. Dataset differences from means for all listed variables are found in the third and fourth columns of Appendices A through E. These difference from mean figures were created using a red blue colormap and specific function code (Auton 2023). Within all of the plots mentioned directly

above, isopycnals were calculated using TEOS-10 following input of conservative temperature and absolute salinity. When isopycnals were included in figures, isopycnal values were subtracted by 1000 to ensure the numbers were legible in each figure.

### 2.2.2 Water mass Identification

For all datasets where CTD data was gathered, individual nutrient data was plotted on axes of potential temperature and salinity with CTD potential temperature and salinity plotted continuously for each cast. Potential temperature and salinity data corresponding to nutrient samples was gathered from in-situ bottle sampling of temperature and salinity. These plots were utilized to observe general nutrient trends in the potential temperature-salinity space for each dataset and to ensure that there were no obvious errors with the nutrient data. Errors in the data were apparent if potential temperature and salinity points for nutrient data were not similar to CTD potential temperature and salinity for the same cast location.

After determining that nutrient data for these datasets was suitable, nutrient data was separated by inner and outer shelf areas, and plotted against potential temperature and salinity. Using known polar and AW water mass characteristics for those applicable to the region of these datasets and with the knowledge that PSW was not present in this region based on 2004 data (Sutherland and Pickart, 2008), AW and POLW were identified within these plots and nutrient data for each water mass was identified. POLW is designed to encompass the characteristics of both PSW and PSWw. Therefore, water mass definitions were derived from the following sources: AW (potential density: Pérez-Hernández et al., 2017 and Dodd et al., 2012; salinity and potential temperature: Sutherland and Pickart, 2008), POLW (potential temperature: evaluated from Rudels et al. 2005; salinity: evaluated from Pérez-Hernández et al. 2017) and can be found in Table 2. Separating nutrient concentrations by each water mass aided in identifying general

trends of nutrient concentrations found, so that comparisons to literature could be drawn. The mean and standard deviation of each nutrient in each water mass in both shelf sections was evaluated individually within each dataset. These calculations for each dataset, water mass, and shelf section were each utilized to create an overall mean and standard deviation for all datasets by evenly taking the average of all means and calculating a standard deviation from those averaged means. Using this overall mean and standard deviation for each nutrient, water mass, and shelf section encompassing all the datasets, corresponding 95% confidence intervals were calculated for each nutrient, water mass, and shelf section. Nutrient concentrations within each water mass were further evaluated by assessing changes with time. Results of all dataset's means, standard deviations, and confidence intervals can be found in Section 3.4 of this study.

**Table 2:** Water mass definitions based on potential density ($\sigma_\theta$, kg/m$^3$), salinity (S, ppt), and potential temperature ($\theta$, °C).

| **Water mass** | **Definition** |
|---|---|
| AW | $\sigma_\theta \geq 1027.6$, S ~ 34.8-35.1, $\theta$ ~ 4.5-6.5 |
| POLW | $32.5 \leq S \leq 34$, $\theta \leq 2$ |

### 2.2.3 Fractions of Pacific Water and Pacific Freshwater

With the various currents (EGC, EGCC, IC) occupying this region of study and due to processes of general Arctic Ocean oceanography, seawater samples gathered in the research area have two main large-body sources: PW and AW. Due to biological processes of denitrification and nitrogen fixation on Pacific source water during its transit through the Bering Strait and Arctic Ocean, PW is easily identifiable from AW by its nitrate to phosphate relationship. PW is reported to have lower nitrate concentrations compared to phosphate and as a result, this relationship can be used to determine the relative amount of PW in a sample to within ± 10% (Jones et al., 1998; Jones et al., 2003). To calculate the fractions of PW and later, PFW for each

sample, similar methods to Jones et al. (2008b), Sutherland et al. (2009), and de Steur et al. (2015) were used by utilizing the known relationship between concentrations of nitrate and phosphate in waters with either AW or PW origin. These relationships are provided in the form of a specific slope and intercept for both types of source water and can be found in Table 3 displayed later in this subsection.

The below equations were used to determine the fraction of PW contained within each sample to an accuracy of ± 10%. Given this study aims to identify the fraction of PW in the POLW by dataset, only data within the POLW parameters was utilized for these calculations. If a specific dataset did not contain any amounts of POLW, then the fraction of PW for samples in that dataset were not calculated. The variables denoting *AW** represent AW together with river water and sea ice meltwater. In Jones et al. (2008b), salinity is used to separate sea ice meltwater and river water from PW, while total alkalinity is used to distinguish river water from sea ice meltwater. In Sutherland et al. (2009), delta $^{18}O$ is also used as a tracer for sea ice meltwater. Rather than separating these two additional sources with additional data and because both have nitrate to phosphate relationships similar to AW (Jones et al., 2003), calculations were only performed for source waters of PW and AW*.

$$\boldsymbol{PO_4^{PW} = PW_{slope}\, x\, NO_3^{PW} + PW_{intercept}} \qquad (5)$$

$$\boldsymbol{PO_4^{AW^*} = AW^*_{slope}\, x\, NO_3^{AW^*} + AW^*_{intercept}} \qquad (6)$$

$$f_{PW} = \frac{\boldsymbol{PO_4^m - PO_4^{AW^*}}}{\boldsymbol{PO_4^{PW} - PO_4^{AW^*}}} \qquad (7)$$

In Equations (5) and (6), $PO_4^{PW}$ and $PO_4^{AW*}$ are the phosphate values the sample would have if it were purely of PW or AW origin, respectively. Similarly, $NO_3^{PW}$ and $NO_3^{AW*}$ are the nitrate values located along each of the same source water regression lines corresponding to

$PO_4^{PW}$ and $PO_4^{AW*}$, respectively, denoting the nitrate values the sample would have if it were purely of PW or AW origin. The respective slopes ($PW_{slope}$ and $AW*_{slope}$) and intercepts ($PW_{intercept}$ and $AW*_{intercept}$) associated with each of these two regression lines for PW and AW were retrieved from Dodd et al. (2012), and can be found in Table 3 below. For Equation (7), to calculate $PO_4^{PW}$ and $PO_4^{AW*}$ used in the formula, $NO_3^{PW}$ and $NO_3^{AW*}$ from the respective Equations (5) and (6) were substituted for nitrate values of the samples found in each dataset. Substituting these variables permitted calculation of the respective phosphate values of the samples using the applicable source water phosphate to nitrate relationship to determine the concentration of phosphate in both source waters. Using these known relationships and Equation (7), the calculated values of $PO_4^{PW}$ and $PO_4^{AW*}$ were used with the concentrations of measured phosphate values from each dataset ($PO_4^m$) to calculate the fraction of PW ($f_{PW}$) in each sample. Where applicable, values of $f_{PW}$ are displayed via an array of boxplots categorized by dataset and shelf location within section 3.5 of this study. Each dataset's and shelf area's mean were calculated and can be found in Table 6.

After calculating the fraction of PW of each dataset's sampling of nitrate and phosphate within the POLW water mass, these values were used to calculate the fraction of PFW for each sample using Equation (8). In the below, the additional variables used to calculate the fraction of PFW ($f_{PFW}$) are the salinity of Atlantic source water ($S_{AW}$) and the salinity of Pacific source water ($S_{PW}$). Both salinity values were gathered from Dodd et al. (2012) and are listed in Table 3. In previous studies, this fraction is used in comparison with fractions of other freshwater sources like meteoric water and sea ice melt. However, the means to calculate these other fractions were not available in this study, so the fractions of PW for all datasets will be compared to literature

values in southeastern Greenland and in the Denmark Strait, an oceanic strait between Greenland and Iceland approximately 400 miles northeast of this study's region.

$$f_{PFW} = f_{PW} \, \boldsymbol{x} \, \frac{\boldsymbol{S_{AW} - S_{PW}}}{\boldsymbol{S_{AW}}} \qquad (\mathbf{8})$$

Within Table 3 below, the respective variables are used to distinguish both PW and AW in the Arctic Ocean. However, these same values can be used to characterize both PW and AW passing through Fram Strait and further south in this research study, as waters exiting Fram Strait are likely a mixture of water from these different source water's pathways. Therefore, from Dodd et al. (2012), AW variables in Table 3 are representative of all water entering the Arctic Ocean from Greenland to Severnaya Zemlya, an archipelago north of Russia and northeast of both the Barents and Kara Seas. The AW slope and intercept values were calculated using data from 2005 to 2011 within the Fram Strait with a potential density greater than 27.60 kg/m$^3$, as less dense samples could contain a PW signature (Dodd et al., 2012). Table 3's PW variables are representative of all water entering the Arctic Ocean through the Bering Strait. The PW salinity value was determined using data from three moorings near the bottom within the Bering Strait from the years 1990 to 2004. Finally, the PW slope and intercept values were adopted by Dodd et al (2012) from values published in Jones et al. (2008a), which used data collected between August to September 2005 that originated from the Canada Basin with salinities between 32 and 33.1 and nitrate concentrations of greater than 1 µmol/kg, ensuring source water measurements did not include waters that experienced denitrification (Jones et al., 2008a; Dodd et al., 2012).

**Table 3:** Slope, intercept, and salinity values utilized in Equations (5), (6), and (8) depicting source waters of PW and AW. The below values were gathered from Dodd et al. (2012).

| | **$PO_4$ v. $NO_3$ slope** | **$PO_4$ v. $NO_3$ intercept** | **Salinity (ppt)** |
|---|---|---|---|
| **Pacific source water (PW)** | 0.0653 ($PW_{slope}$) | 0.94 ($PW_{intercept}$) | 32 |
| **Atlantic source water (AW)** | 0.053 ($AW^*_{slope}$) | 0.17 ($AW^*_{intercept}$) | 34.9 |

Similar to procedures conducted for fractions of PW, where applicable, values of $f_{PFW}$ are displayed via an array of boxplots categorized by dataset and shelf location within section 3.5 of this study. Each dataset's and shelf area's mean were calculated and can be found in Table 6.

### 2.2.4 Nutrient-to-nutrient relationships

Besides using the relationship between nitrate and phosphate to determine the fractions of PW and PFW in the POLW water mass, examining other nutrient-to-nutrient relationships is equally useful in this study. These other nutrient-to-nutrient relationships were also examined to assess the differences between in-situ observations occurring amongst both shelf sections and the Redfield-Brzezinski ratio. As stated previously, in-situ ratios typically vary from the accepted ratios depending on several factors. To evaluate these potential differences, plots of nitrate versus phosphate, nitrate versus silicate, and silicate versus phosphate were created to evaluate the N:P, N:Si, and Si:P ratios, respectively. For each plot, a linear regression line was fitted to the datapoints. If the samples exhibited the same ratio as is published in the literature (C:Si:N:P = 106:15:16:1), then the regression slopes for each plot would be equivalent to the ratios, meaning nitrate versus phosphate would have a slope of 16, nitrate versus silicate would have a slope of 1.07, and silicate versus phosphate would have a slope of 15. The respective y-intercepts for each plot were also utilized to draw conclusions about how some nutrients may be more limiting than others in this particular environment. If data did not exhibit a linear trend for a

range of nutrient values, this information was also utilized to draw conclusions about the interactions of nutrients in the region of study.

CHAPTER 3: RESULTS & DISCUSSION

## 3.1 Mean CTD Potential Temperature and Salinity distributions inshore and offshore

Mean interpolated plots presented in this section and the next are representative of an average of the following datasets: 2002b, 2004, 2006, 2008a, 2010a, 2012, 2014, and 2016a. Details on selection of these datasets are contained in subsection 2.2.1 of this study. The mean plots in Figures 5 through 9 within this section and section 3.2 were configured using the interpolated fields of each dataset, found in the first two columns of Appendices A through E. The data were quality controlled and a limited number of casts were eliminated on the basis of unphysical differences with the neighboring data. In all mean plots within this section and the next (Figures 5 through 9), density is represented as density anomalies. Below, Figure 5 illustrates the mean CTD potential temperature of these datasets for both shelf sections, and later in this section, Figure 6 details the mean CTD salinity for both shelf sections.

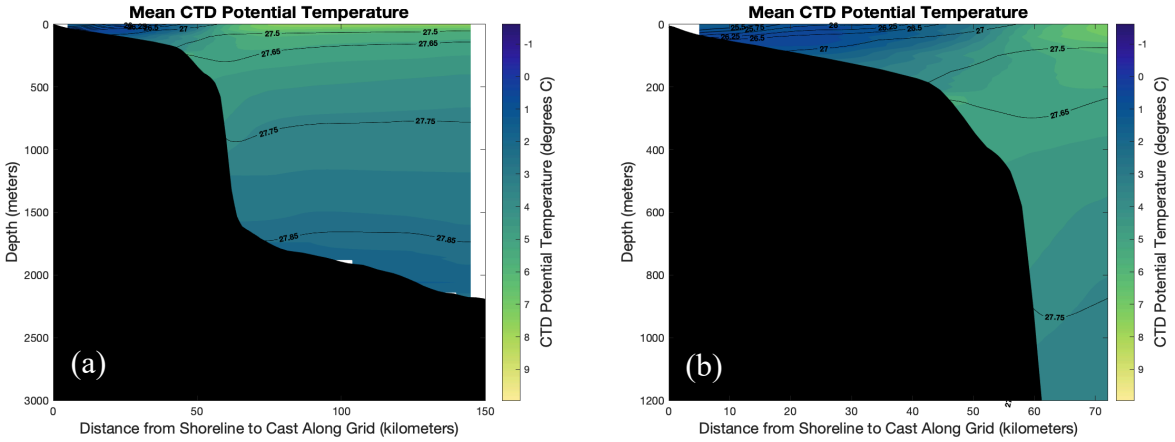


**Figure 5:** Mean CTD potential temperature for (a) both shelves and (b) inner shelf only using datasets 2002b, 2004, 2006, 2008a, 2010a, 2012, 2014, and 2016a. The solid black lines denote mean isopycnals in kg/m$^3$.

General distribution of properties for the summer months of 2002 to 2016 indicate that colder, lower-salinity waters exist at the surface closest to the shoreline with lowest temperatures and salinities closest to the surface and furthest inshore. Further offshore beyond the continental

slope, temperatures exhibit similar general spatial distribution to other open-ocean regions, where waters are warmer at the surface, gradually decrease in temperature with depth, and are coldest at the bottom. Temperature distribution furthest inshore is likely the product of both runoff from glaciers in the region and further north along the eastern coast of Greenland, in addition to transport of polar-origin waters carried via the EGCC/EGC system. Within the inner shelf section and in temperatures measured closer to the surface, waters exhibit a non-linear increase in temperature from the shoreline to off shore. At the surface, temperatures range from below freezing or freezing at 5 km distance to 2.5ºC at 45 km to 5ºC at 58 km to eventually, a sustained high of 7.5ºC at 75 km. This warming is due to both surface heating and less EGC influence further offshore. Salinity at the surface experiences a similar non-linear increase due to similar effects.

Besides the influences of the EGCC/EGC system on the difference in temperatures closer to the surface, another notion may explain the differences in temperature exhibited offshore and at depth. Water masses are known to transport nutrients and contain specific concentrations depending on their respective origin and circulation. According to García-Ibáñez et al. (2015) from data between 1997 – 2010, in this region and beyond the Greenland slope, there exists the following water masses: IrSPMW (surface-1000 m), LSW (1000-2000 m, primarily), and ISOW (1800 m-bottom). Within that study, each were characterized by the following potential temperature and salinity specifications: IrSPMW (5.00 ± 0.02 °C, 35.014 ± 0.013 ppt), LSW (3.00 ± 0.19 °C, 34.87 ± 0.02 ppt), and ISOW (2.6 ± 0.08 °C, 34.980 ± 0.003 ppt) [García-Ibáñez et al., 2015]. Using these same specifications, the first two water masses are identifiable in Figure 5 (a) at the following depths: IrSPMW (200-250 m at 140 km distance and 300-450 m at 60 km distance) and LSW (1000-1800 m across all distances). For waters below 1800m, ISOW

is likely mixed with LSW, as the potential temperature range within these waters is between what would be expected for each, inferring mixing of the two water masses. Even though IrSPMW and LSW are easily identifiable in this study, we combined them into AW, as doing so allowed for more substantial comparisons to previous studies that reviewed similar variables throughout the eastern Greenland coast.

Transitioning to mean CTD salinity in Figure 6 below and water masses being measured in this study, an isohaline of 34.8 ppt is used as the defining characteristic for AW. The mean plots indicate a constant intrusion of this water mass onto the shelf area at 225 m depth offshore (45 km) and at the surface further offshore (at 73 km). Shown in the first two columns of Appendix B, this signal is present amongst all eight datasets with an intrusion range of 34 to 52 km at depth where the isohaline meets the bottom, and is present at the surface with a range of 53 to 75 km distance from the shoreline. This difference between years could be a result of when the measurements were taken between the different months in different years, but is more likely a result of the changing flux and influence of the EGC from year to year. A similar distribution is described for 2004 (Sutherland and Pickart, 2008). In that study, the EGC/IC front was easily identified as a near vertical isohaline of salinity less than 34.8 ppt that existed from 30 m depth to nearly the bottom (Sutherland and Pickart, 2008). This characteristic is also present in the majority of this study's datasets that have sufficient inner shelf coverage, where the isohaline is nearly vertical from around 20 m depth to around 40 m from the bottom, before the isohaline shifts to an angle to meet the bottom further inshore. However, this characteristic is somewhat lost in the mean salinity plots due to the averaging method used to smooth the salinity contours, but it is still worth noting.

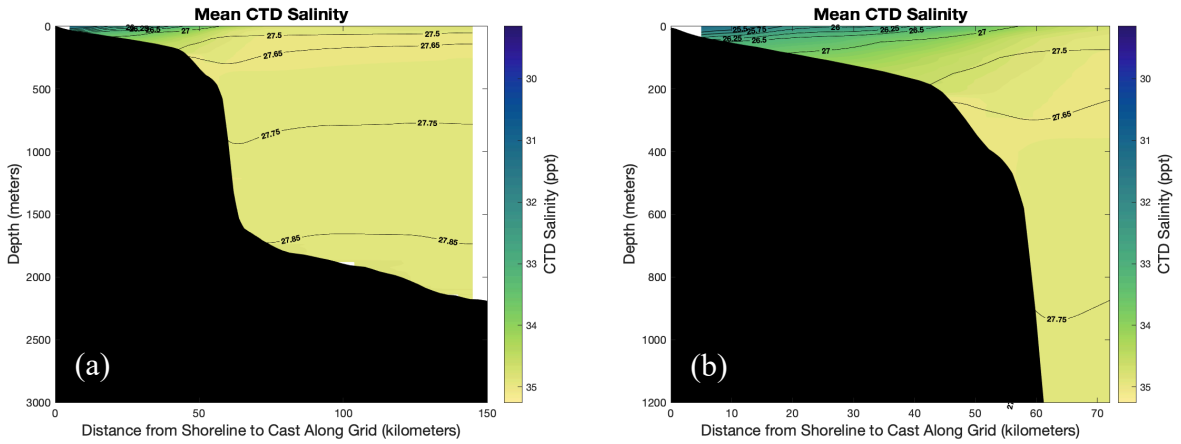


**Figure 6:** Mean CTD salinity for (a) both shelves and (b) inner shelf only using datasets 2002b, 2004, 2006, 2008a, 2010a, 2012, 2014, and 2016a. The solid black lines denote mean isopycnals in kg/m$^3$.

Further inshore of the EGC/IC front, Sutherland and Pickart (2008) noted the presence of the EGCC around 20 km shoreward of the front, in which waters with salinity of less than 32 ppt were exhibited. This trend is very similar to the mean cross sections in this study that had significant inner shelf coverage, indicating the presence of the EGCC throughout almost all of the years between 2002 to 2016, according to CTD potential temperature and salinity distributions. In addition to the phenomenon discussed thus far, another characteristic is noteworthy in this analysis of data. In years 2006 and 2012, waters of lower salinity (< 34.8 ppt) are found at the surface to around 50m depth from around 90 km to 145 km distance from the shoreline, but given this does not occur in the other datasets, this signal is lost in the displayed mean. All open-ocean water masses and mixing between them that were observed within Figure 5 (a) are also present with the same depth ranges within Figure 6 (a).

Several years were characterized by data that was significantly different from all other years. This was the case for 2004's CTD salinity data. Exhibited in Figures 23 (g) and (h) within Appendix B, 2004's difference from the mean is significantly different from that of all other years. The colorbars for mean differences for both CTD temperature (Appendix A) and salinity

are magnified substantially to enhance the differences between datasets. This may indicate a problem with 2004's CTD salinity measurements. Within the same Appendix, 2002b (Figures 23 (c) and (d)) is also quite different from the remaining datasets, in that all depths greater than 200 m indicate water that is fresher than the mean. Although, the differences at all depths are not as stark as 2004, these differences may also indicate a problem with 2002b's CTD salinity measurements. Also noted in 2002b's CTD potential temperature difference plots located in the third and fourth columns of Appendix A (Figures 22 (c) and (d)), colder water than the mean across almost all depths throughout the cross section produces a distribution that is noticeably different from the other datasets, which display variable differences from the mean throughout depths and distances within the grid. Seeing as how these datasets still had significant shelf coverage and spanned the earlier portion of this study with nutrient data, datasets 2002b and 2004 remained in order to analyze nutrient differences and other variables analyzed in this study, as it was concluded that the data was useful in comparison to later years.

### 3.2 Mean nutrient distribution inshore and offshore

In reviewing mean nutrient distributions, it is evident that each nutrient experiences similar distribution from inshore to offshore and surface to bottom throughout the cross section. Generally, Figures 7 through 9 below indicate low to zero nutrient presence at the surface across the whole cross section and an increase at depth. However, the manner by which each nutrient's concentration increases by depth is different. Reviewing the plots for the inner shelf section only (Figures 7 (b), 8 (b), and 9 (b)) reveals that waters furthest inshore exhibit low or no nutrient concentrations and these concentrations gradually increase in a step-like manner, increasing evenly both with depth and distance from the shoreline. These steps (0.75 μmol/kg for both nitrate and silicate and 0.1 μmol/kg for phosphate) are spaced closer towards the surface and

inshore and slowly widen with distance from the shoreline. Further offshore, these steps either stop increasing (i.e. nitrate and phosphate) or continue widening and increasing in concentration with depth and distance (i.e. silicate). Beyond the continental slope, higher concentrations for all nutrients exist further offshore.

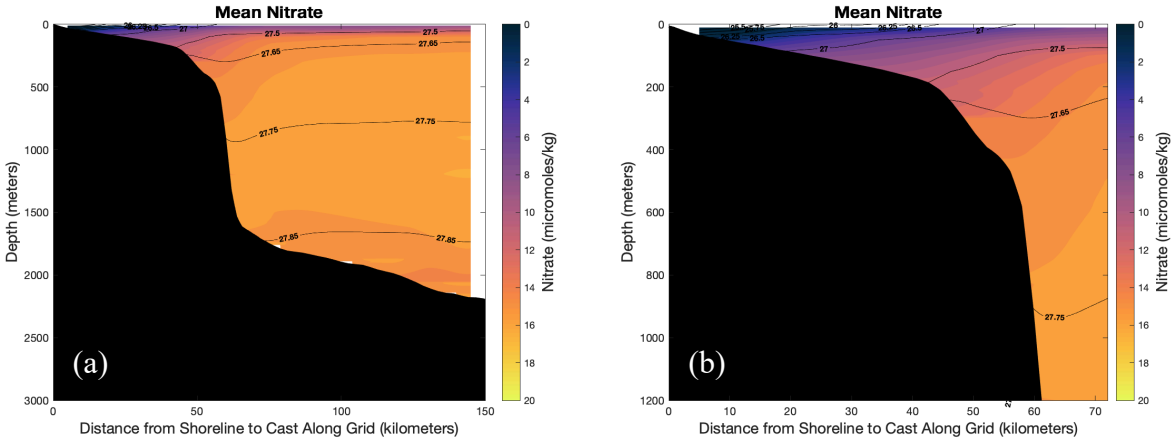


**Figure 7:** Mean nitrate concentration for (a) both shelves and (b) inner shelf only using datasets 2002b, 2004, 2006, 2008a, 2010a, 2012, 2014, and 2016a. The solid black lines denote mean isopycnals in kg/m$^3$.

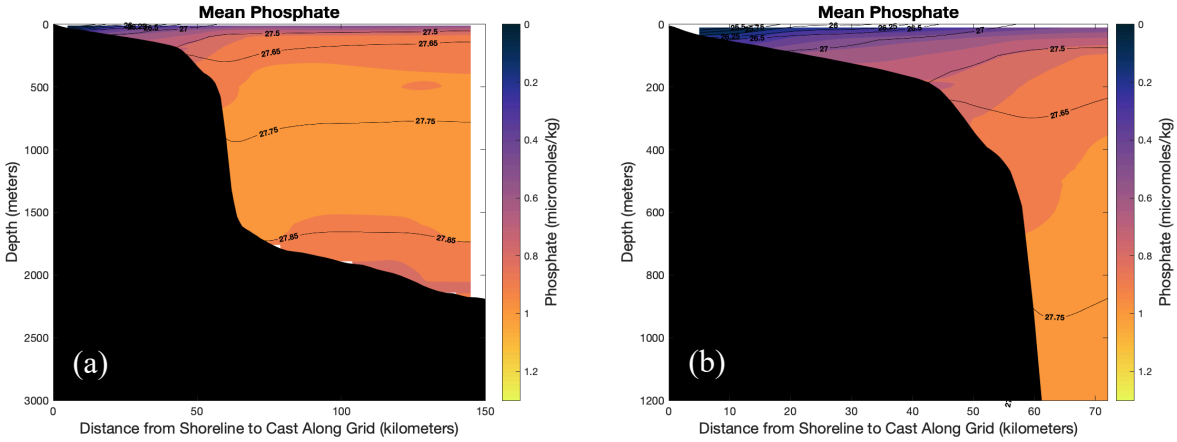


**Figure 8:** Mean phosphate concentration for (a) both shelves and (b) inner shelf only using datasets 2002b, 2004, 2006, 2008a, 2010a, 2012, and 2016a. The solid black lines denote mean isopycnals in kg/m$^3$.

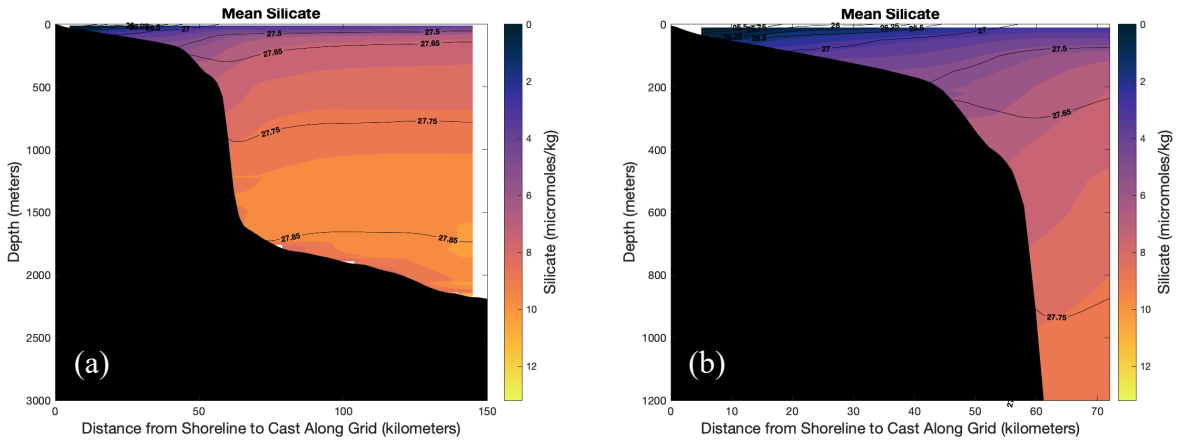


**Figure 9:** Mean silicate concentration for (a) both shelves and (b) inner shelf only using datasets 2002b, 2004, 2006, 2008a, 2010a, 2012, 2014, and 2016a. The solid black lines denote mean isopycnals in kg/m$^3$.

In the euphotic zone where light penetrates the surface waters enough to allow photosynthesis to occur, nutrients are utilized for growth and photosynthesis quicker than they can be replenished. Therefore, it is not a surprise that the upper 80 m across all distances exhibits this same distribution. However, furthest offshore, it is surprising to see that both nitrate and phosphate level off and have a large portion of their respective cross sections with higher nutrient concentrations in the middle depths (250-1800 m for nitrate and 500-1700 m for phosphate) where it does not change. This area is exhibited in silicate too, but only exists much deeper from 1000-2000 m. These areas have the highest nutrient concentrations of all depths, as concentrations decrease from these levels closer towards the bottom and in the benthic environment. Beyond the continental slope, this area within the middle depths of each plot likely exists due to the presence of open-ocean water masses, discussed later in this section. In addition to water mass intrusion, the differences in where these middle depths start (i.e. 250 m for nitrate, 500 m for phosphate, and 1000 m for silicate) is likely also a product of the organisms using these nutrients (e.g. bacteria absorb nitrate and phosphate in the dark) and how quickly they can be replenished at various depths by bacteria remineralization. More organisms demand nitrate

and phosphate than silicate and/or there is more silicate present than is needed. With the above depths in mind, the notion stated earlier that nitrate is often the most limiting nutrient in the North Atlantic, followed by phosphate, and then, silicate (Moore et al., 2013) is demonstrated here.

Just as open-ocean water masses were identified in the previous section of this study, the same process is applied to nutrient concentrations. Given IrSPMW is seen from 200-450 m, LSW exists between 1000-1800 m, and ISOW is observed to be mixing with LSW below 1800 m, it is likely that these water masses are transporting nutrients that have been circulated within each respective water mass. As measured by García-Ibáñez et al. (2015), the mean nitrate, phosphate and silicate for IrSPMW is 15.0, 0.98, and 7.1 μmol/kg, respectively. The same nutrients for LSW are 16.5, 1.05, and 10.0, respectively, and for ISOW: 15.5, 1.2, 10 (García-Ibáñez et al., 2015). All of the nutrient concentrations for all three water masses are fairly similar to those observed in this study with the exception of phosphate in ISOW, which has a literature value that is higher than observed values in this study. This is likely due to the fact that phosphate concentrations are so small in concentration and may be difficult to identify errors as a result. Even if phosphate is recorded in error at depth, enough evidence is present in this study to determine the presence of the above three water masses in southeastern Greenland from 2002 – 2016, the last of which (ISOW) is likely mixed with LSW at depth. Given this study identified and considered AW and POLW only, the three water masses discussed above will not be mentioned further in this Chapter.

Just as CTD temperature and salinity differ between datasets, some pronounced interannual differences were observed for nitrate and phosphate (Appendix C). For nitrate, 2014 has anomalously low values from the mean throughout the water column. There is potentially an

error with this dataset's nitrate data. Both 2002b and 2006 exhibited increased nitrate throughout the water column, but these differences from the mean are not extreme. Similar to 2004's data, 2006 has staggered cast locations that form two distinct hydrographic lines over the continental slope (as observed in Figure 3 previously in this study), which may have contributed to this appeared increase. Additionally, 2010a has an increased nitrate difference from the mean for all depths greater than 200 m, but again, these differences are not extreme. Outside of 2014, all of the above datasets may have data that is anomalous that could have been linked to less nitrate demand by organisms or an increase in nitrate transport, or perhaps, there are errors in the datasets. Further conclusions cannot be drawn from the available data.

Phosphate differences from the mean, which are located in the third and fourth columns of Appendix D, are largely variable by depth and distance for most of the datasets. However, 2004 has anomalously high phosphate throughout the water column and 2008a has anomalously low phosphate throughout the water column. It is unsure whether these signals are false or if these differences really exhibited natural phenomenon. However, mentioned previously, phosphate concentrations are so small that it is possible these values were measured in error. Again, just as before, it was determined that viewing all of these datasets as part of the mean was important to explain the differences between datasets over the years examined. From these summer observations of southeastern Greenland nutrients from 2002 – 2016, no significant trend in interannual variability is observed.

Similar to both nitrate and phosphate, silicate differences from the mean are also largely variable by depth and distance, and display no significant trends in interannual variability. Located in the third and fourth columns of Appendix E, these differences from the mean silicate

distribution and any indicated anomalies do not favor any particular dataset. All datasets show variability, but no particular dataset can be singled out as an anomalous year.

### 3.3 Potential Temperature-Salinity diagrams for all datasets and nutrients

Another useful oceanographic tool used in this study are temperature-salinity plots. Figures 10 (a) and (b) below list all bottle potential temperatures and corresponding salinities colored by dataset for both the inner and outer shelf sections. All plots in this section denote AW and POLW water masses by a blue triangle and box, respectively. From these plots, it is evident that the POLW water mass only exists within the inner shelf section. This section has data that spans the lowest salinities, which is not surprising, especially given the mean CTD salinity plots indicated the coldest and freshest waters furthest inshore. The data between the AW and POLW water masses indicate various stages of mixing between the two water masses. Conversely, the outer shelf contains water that exhibits a much smaller range of salinities where no waters of polar-origin are noted. Given each data point has an associated nutrient concentration, nutrient trends by water mass are examined later in this study.

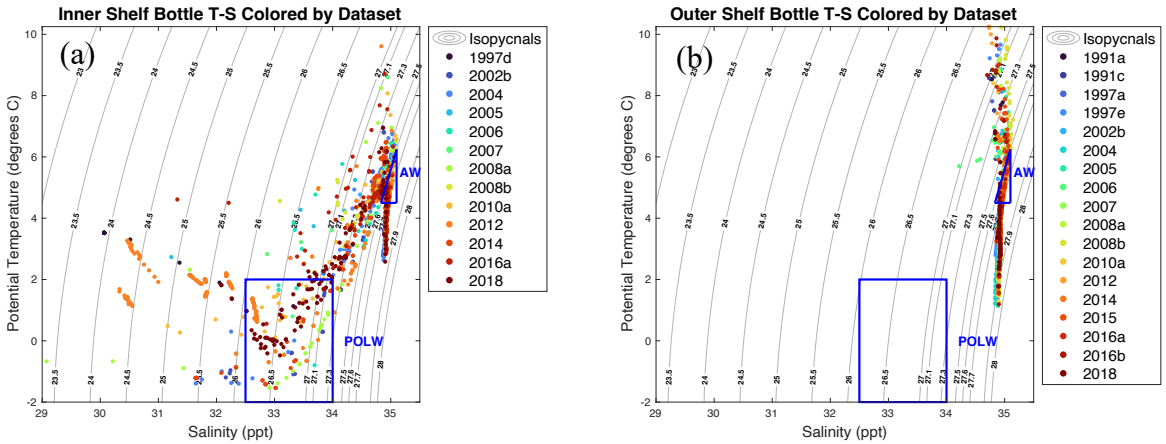


**Figure 10:** Potential temperature versus salinity colored by dataset. This plot includes all datasets within both the (a) inner and (b) outer shelves, respectively. The solid black lines denote mean isopycnals in kg/m$^3$. The blue triangle and rectangle denote the AW and POLW water masses, respectively.

Below, Figures 11 through 13 illustrate how nutrient distribution differs within each section and water mass. For these plots, the boundaries on each axis are decreased to allow for the best visual representation of the data. Plots containing the full temperature and salinity ranges of all samples for both shelf sections can be found in Appendix F. Similar to the previous figures above, both water masses are annotated in the same manner below and within the Appendix.

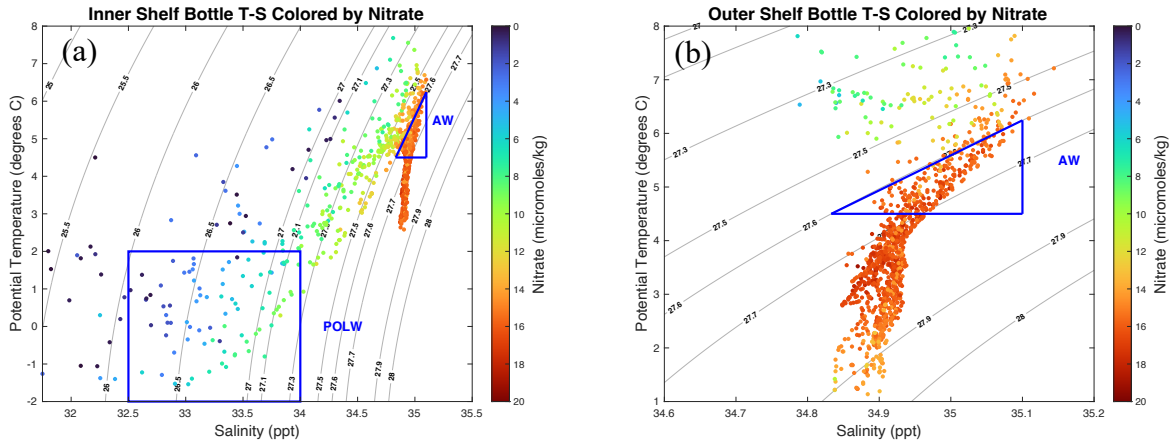


**Figure 11:** Potential temperature versus salinity colored by nitrate with range magnified for detail. This plot includes all datasets within both the (a) inner and (b) outer shelves, respectively. The solid black lines denote mean isopycnals in kg/m$^3$. The blue triangle and rectangle denote the AW and POLW water masses, respectively.

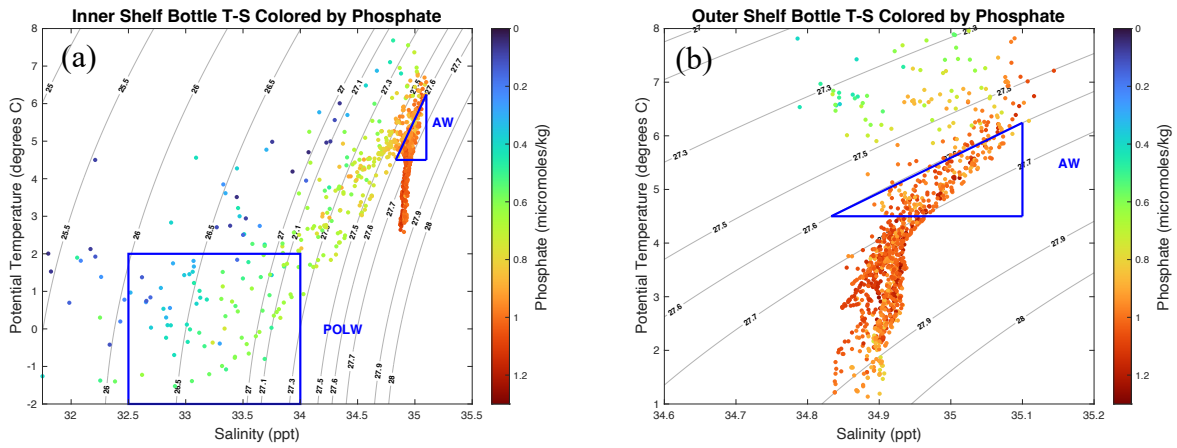


**Figure 12:** Potential temperature versus salinity colored by phosphate with range magnified for detail. This plot includes all datasets within both the (a) inner and (b) outer shelves, respectively. The solid black lines denote mean isopycnals in kg/m$^3$. The blue triangle and rectangle denote the AW and POLW water masses, respectively.

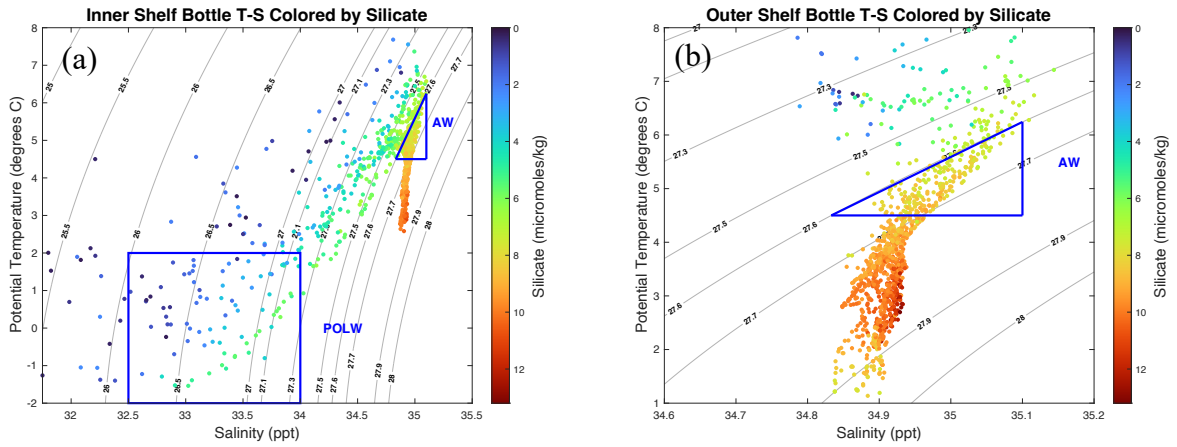


**Figure 13:** Potential temperature versus salinity colored by silicate with range magnified for detail. This plot includes all datasets within both the (a) inner and (b) outer shelves, respectively. The solid black lines denote mean isopycnals in kg/m$^3$. The blue triangle and rectangle denote the AW and POLW water masses, respectively.

In each inner shelf section (Figures 11 (a), 12 (a), and 13 (a)), the POLW water mass is characterized by nutrient-depleted samples when compared to the AW water mass. From the plots alone, the nutrient concentrations within the POLW box span a wider range of values than those of AW, indicating that the colder and fresher waters become nutrient-depleted at different rates or a replenishment has taken place in some areas but not others within this water mass. Also

exhibited within each plot of the inner shelf section is a distinct range of salinities and temperature values that are host to near-zero nutrient concentrations. These values are found in the top left corner of each POLW box and are in addition to samples that are both fresher with similar temperatures (to the left of the POLW box) and samples with the same salinity but have a greater temperature (above the POLW box). These samples are likely at the surface or are furthest inshore at shallow depths. Within the inner shelf plots, the space between the water mass areas in the temperature-salinity plots is host to nutrient concentrations of a large range, which indicates mixing. However, between the three nutrients, silicate appears to have the smallest range with samples of smaller concentration closer to the AW box. This increase in the number of samples with lower silicate concentrations is comparable to the mean silicate plots discussed earlier in section 3.2. Mixing that occurs in this boundary between water masses within these diagrams likely occurs in the area that is delineated by a near vertical isohaline from just below the surface to just above the bottom, as discussed in section 3.1 of this study. This large range can be attributed to the dynamic mixing of AW between years, the influence that this water mass has on nutrient concentrations, and the effect of upwelling of nutrient-rich waters in these samples.

In the magnified plots of the outer shelf section (Figures 11 (b), 12 (b), and 13 (b)), the increased nutrient concentrations within the AW water mass are certainly clear. The difference between the higher nitrate and phosphate concentrations compared to the silicate concentrations in the same temperature and salinity range is also clearly seen. The differences in AW nutrient concentrations between shelf sections appears small and is confirmed by the 95% confidence intervals found in Table 4 within the next section of this study. Finally, in the plots of the outer shelf section, below the AW triangle at around 2.8ºC and approximately 34.88 ppt, the

temperatures and salinities of the samples bow in, leaving an area where no samples occur relative to the rest of the samples plotted in this area. After examining the same area in the inner shelf section, this bowing was not as defined or non-existent, given fewer samples with temperature and salinity in this range within that area. This bowing in the outer shelf is likely attributed to a flux of saltier waters in this temperature range due to the AW intrusion onto the shelf, but this cannot be confirmed by other plots and remains speculation.

### 3.4 Water mass nutrient content variability

Examined above, it is clear that both AW and POLW water masses experience different nutrient concentrations. Within Table 4 below, each nutrient's concentration is denoted by the mean, standard deviation, number of observations by individual dataset (in parenthesis), and 95% confidence interval (denoted in bold). This table delineates each water mass by the respective shelf location. Given POLW was not found in samples from the outer shelf, this table only lists values from the inner shelf for this water mass. Utilizing a confidence interval to evaluate the data is important, as it provides a 95% probability that the true value falls within this range of values. With greater than 30 samples to account for in each section, water mass, and nutrient type, the below confidence intervals are provided with great conviction in their ranges.

**Table 4:** Nutrient mean and standard deviation for all dataset's biogeochemical observations separated by inner and outer shelf sections. The number next to the standard deviation is the number of dataset observations in parenthesis. Below each mean, standard deviation, and number of dataset observations, the bolded numbers in parenthesis are the 95% Confidence Intervals for each grouping. All units are μmol/kg.

| | **AW (inner)** | **AW (outer)** | **POLW (inner)** |
|---|---|---|---|
| **$NO_3$** | 15.16 ± 0.50 (9)<br>**(14.78, 15.54)** | 15.84 ± 0.40 (18)<br>**(15.64, 16.04)** | 5.02 ± 1.55 (11)<br>**(3.98, 6.06)** |
| **$PO_4$** | 0.98 ± 0.03 (8)<br>**(0.95, 1.01)** | 1.01 ± 0.03 (16)<br>**(0.99 1.03)** | 0.51 ± 0.08 (10)<br>**(0.45, 0.57)** |
| **$Si(OH)_4$** | 7.80 ± 0.46 (9)<br>**(7.45, 8.15)** | 8.17 ± 0.40 (17)<br>**(7.96, 8.38)** | 3.10 ± 0.65 (11)<br>**(2.66, 3.54)** |

In contrast to previous studies that reviewed nutrient concentrations within water masses AW, PSW, and PSWw, these confidence intervals vary slightly. This has a lot to do with the location of previous studies and how each water mass was defined. In this study, AW is defined by potential temperature, salinity, and potential density, while POLW is a water mass unique to this study and designated by potential temperature and salinity for the purposes of capturing trends of both PSW and PSWw, given the research area and the presence of both water masses observed in this study. Even though both water masses in this study are defined slightly differently from published literature, it is still reasonable to compare results with other studies. Due to circulation of surface currents and water masses in Fram Strait, it is important to mention again that western Fram Strait exports polar-origin waters from the Arctic Ocean and eastern Fram Strait imports AW into the Arctic Ocean. Given the location of this study and that waters examined here were once exported through the western side of Fram Strait, results from western Fram Strait should be held in greater regard than those from the eastern Fram Strait.

Numerous studies have reviewed nutrient flux and transport through western Fram Strait, but the only study that has reviewed nutrient concentrations by water mass in the area was Tuerena et al., 2021 who reviewed data from 2016 and 2018. In that study, AW was defined as $\theta > 2$ºC and 1027.7 kg/m$^3$ $\leq \sigma_\theta \leq$ 1027.97 kg/m$^3$, or S > 34.92 ppt and $\sigma_\theta <$ 1027.7 kg/m$^3$, and PSW was defined as $\theta < 0$ ºC and $\sigma_\theta <$ 1027.7 kg/m$^3$. Nutrient concentrations in PSWw were not quantified. Nitrate and silicate mean and standard deviations were calculated for both water masses, but phosphate was not calculated in this study. These values are found in Table 5 below and are labeled as Tuerena et al., 2021 for each applicable nutrient and water mass. Given Tuerena et al. (2021) did not compute phosphate concentrations in the water masses and did not include PSWw in analysis, another study by Duarte et al. (2021) is utilized for comparison. In

that study, data spanning from 1972-2016 northeast of Fram Strait defined PSWw as $\theta > 0^{o}C$ $\sigma_{\theta} < 1027.7$ kg/m$^3$. Below, Table 5 lists the mean and standard deviations for nitrate and silicate in AW and PSW (from Tuerena et al., 2021), in addition to both the phosphate 95% confidence intervals for AW, PSW, and PSW, and all nutrients' 95% confidence intervals for PSWw (in Duarte et al., 2021).

**Table 5:** Applicable water mass nutrient concentrations for western (Tuerena et al, 2021) and eastern (Duarte et al., 2021) Fram Strait. Concentrations listed for western Fram Strait denote the mean and standard deviation. Those listed for eastern Fram Strait provide the 95% confidence interval.

| | **AW** | **PSW** | **PSWw** |
|---|---|---|---|
| **$NO_3$ (Tuerena et al., 2021)** | 11.6 ± 0.8 | 7.2 ± 2.3 | |
| **$NO_3$ (Duarte et al., 2021)** | | | (4.52, 5.14) |
| **$PO_4$ (Tuerena et al., 2021)** | | | |
| **$PO_4$ (Duarte et al., 2021)** | (0.81, 0.83) | (0.55, 0.57) | (0.35, 0.41) |
| **$Si(OH)_4$ (Tuerena et al., 2021)** | 7.1 ± 0.7 | 1.4 ± 2.7 | |
| **$Si(OH)_4$ (Duarte et al., 2021)** | | | (2.03, 2.63) |

When comparing the above literature values to those calculated in this study, concentrations are quite different between the two. This is likely due to the differences in sample locations. For literature values published in Tuerena et al. (2021), nitrate and silicate values for the AW water mass are smaller and similar than this study's results, respectively. In the same study for the PSW water mass, published values for nitrate and silicate are larger and smaller than this study's results, respectively. This study's differences when compared to Tuerena's results are likely due to the AW influence fed directly via the IC and a general difference in water mass defining characteristics between the two. For results published in Duarte et al. (2021), the phosphate confidence intervals were lower for AW, similar for PSW, and lower for PSWw. For results in the PSWw water mass, the confidence intervals for nitrate and silicate were similar and lower when compared to this study's POLW values, respectively. These differences are likely attributed to how water masses were defined and the location of those

samples, as Duarte's results were characterized by water flowing into the Arctic Ocean, rather than measurements of exported waters, like those in this study. These differences were expected and are interesting to observe between published values and discovered values in this study.

In Figures 14 through 16 below, box and whiskers plots detail nitrate, phosphate, and silicate concentration ranges for AW amongst both shelf sections. Each dataset's boxplot denotes the 25$^{th}$ and 75$^{th}$ percentiles, median, and data points not considered outliers. Those considered outliers are marked with a red plus sign. The mean nutrient concentration for each dataset is represented by a blue shaded diamond and the applicable 95% confidence interval is represented by two dashed horizontal green lines above and below the solid horizontal green line, which denotes the applicable mean. The below plots illustrate that nitrate and silicate concentrations remain fairly constant from year to year, as more observations for each dataset likely lead to this consistency in values. This consistency in nitrate is stated with the exception of 2014, which shows a sharp decrease in nitrate within both the inner and outer shelf sections. This dataset's decrease in nitrate values was referenced earlier in section 3.2 and is possibly due to errors in this dataset. Furthermore, demonstrated in the outer shelf plots for all AW nutrient concentrations (Figures 14 (b), 15 (b), and 16 (b)), more datasets are represented for this region of the shelf. This increase in datasets also yields an increase in variability from year-to-year and a larger range between the maximum and minimum respective nutrient values within each plot. Even though the outer shelf confidence intervals are tighter than the inner shelf confidence intervals, this characteristic comes from the number of datasets, not necessarily less variability between them.

Further below, Figure 17 illustrates nutrient concentrations for POLW, which reveals that concentrations are highly variable from year to year. This variability is partly due to the decrease

in observations when compared to AW. Phosphate concentrations for both water masses and shelf sections also share this highly variable characteristic. This variability is most likely due to the small quantity of each phosphate concentration and measurements may be marginally different from natural processes due to this. All variabilities for each nutrient and water mass cannot be compared to previous studies, as no other studies have been conducted in this region.

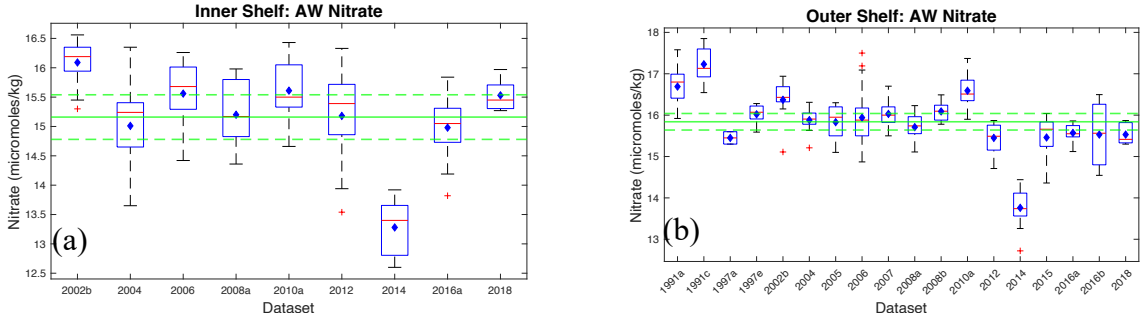


**Figure 14:** Box and whiskers time series plots for AW nitrate concentrations for both (a) inner shelf and (b) outer shelf sections. Each box's bottom and top edges indicate the 25$^{th}$ and 75$^{th}$ percentiles, respectively. The median and mean are represented by the red horizontal line and blue shaded diamond, respectively. The whiskers extend to the data points not considered outliers and all outliers are plotted with the "+" symbol. The mean of all datasets is represented by the solid green line. The upper and lower bounds of the 95% confidence interval for all datasets are represented by the dashed green lines above and below the mean, respectively.

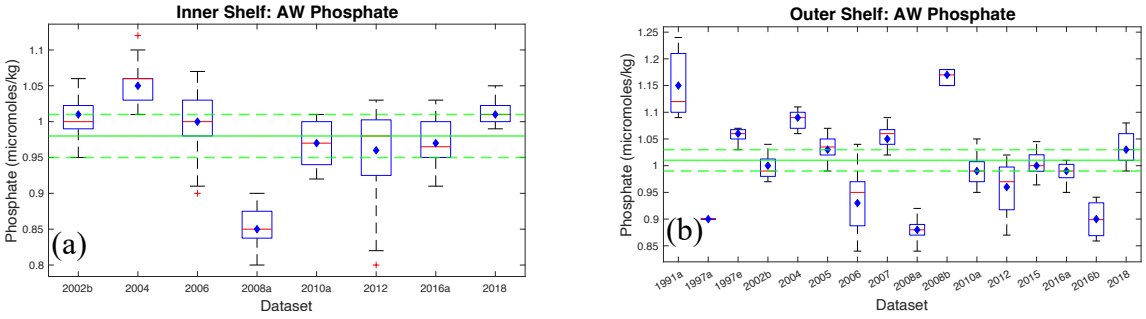


**Figure 15:** Box and whiskers time series plots for AW phosphate concentrations for both (a) inner shelf and (b) outer shelf sections. Each box's bottom and top edges indicate the 25$^{th}$ and 75$^{th}$ percentiles, respectively. The median and mean are represented by the red horizontal line and blue shaded diamond, respectively. The whiskers extend to the data points not considered outliers and all outliers are plotted with the "+" symbol. The mean of all datasets is represented by the solid green line. The upper and lower bounds of the 95% confidence interval for all datasets are represented by the dashed green lines above and below the mean, respectively.

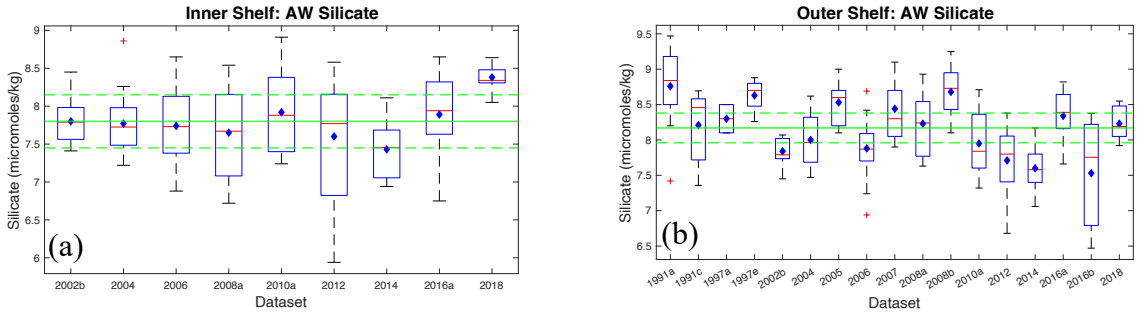


**Figure 16:** Box and whiskers time series plots for AW silicate concentrations for both (a) inner shelf and (b) outer shelf sections. Each box's bottom and top edges indicate the 25$^{th}$ and 75$^{th}$ percentiles, respectively. The median and mean are represented by the red horizontal line and blue shaded diamond, respectively. The whiskers extend to the data points not considered outliers and all outliers are plotted with the "+" symbol. The mean of all datasets is represented by the solid green line. The upper and lower bounds of the 95% confidence interval for all datasets are represented by the dashed green lines above and below the mean, respectively.

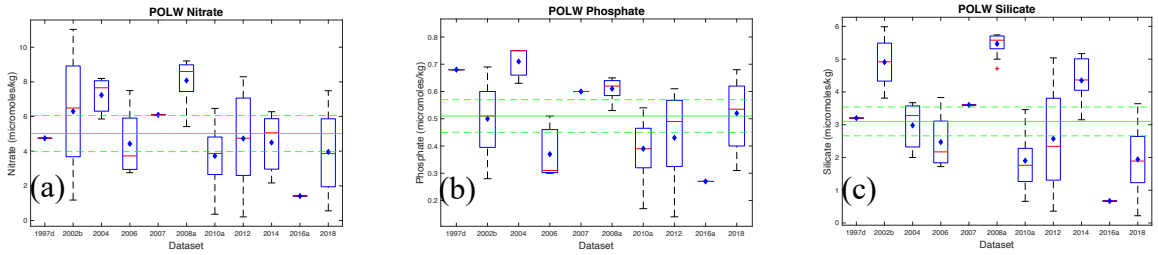


**Figure 17:** Box and whiskers time series plots for (a) nitrate, (b) phosphate, and (c) silicate concentrations in the POLW water mass. Each box's bottom and top edges indicate the 25$^{th}$ and 75$^{th}$ percentiles, respectively. The median and mean are represented by the red horizontal line and blue shaded diamond, respectively. The whiskers extend to the data points not considered outliers and all outliers are plotted with the "+" symbol. The mean of all datasets is represented by the solid green line. The upper and lower bounds of the 95% confidence interval for all datasets are represented by the dashed green lines above and below the mean, respectively.

### 3.5 Fractions of Pacific Water and Pacific Freshwater in Polar Water

Discussed earlier, the relationship between the concentrations of nitrate and phosphate collected in seawater samples can be utilized to determine the fractions of AW and PW in that sample to within a ±10% error. In Figure 18 below, these samples are color coded by dataset and displayed for the POLW water mass located within the inner shelf section. The blue solid line represents the relationship between nitrate and phosphate for a sample of purely AW-origin and

the red solid line represents the same for a sample of purely PW-origin. The blue and red dashed lines represent the ±10% error for each source line, respectively. Following the methods listed in subsection 2.2.4, each sample with corresponding nitrate and phosphate measurements from the same location and depth within the POLW water mass are plotted below. The fractions of PW and PFW were calculated for each sample using these procedures. If a sample was found to the left of the AW source line, it was determined to be of 100% AW-origin. If a sample lied between the two source lines, it was determined to have mixed with PW in some measured capacity. Overall trends indicate that around half of all POLW samples are of AW-origin with the other half having been found to be mixed with PW, which is what this section aims to calculate and discuss.

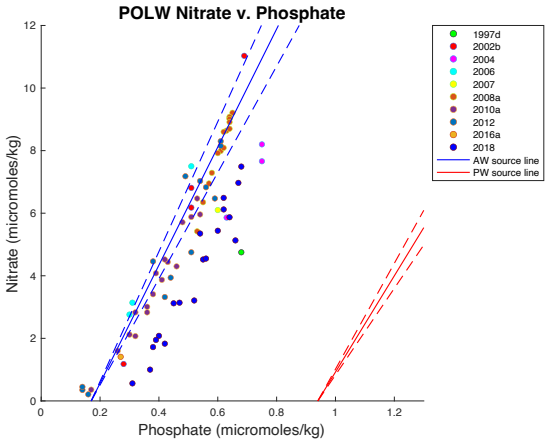


**Figure 18:** Nitrate versus phosphate plot for the POLW water mass. Applicable datasets are plotted by color. Atlantic water and Pacific water source lines from literature values are details as a solid blue and red line, respectively. The blue and red dotted lines represent the ±10% errors for both source lines, respectively.

Using equations (7) and (8) from earlier in this study and data from the POLW water mass, the fractions of PW and PFW were calculated for all applicable data. In Figures 19 (a) and (b) below, box and whiskers time series plots display the fractions of PW and PFW in POLW over the study period, respectively. Each dataset's boxplot denotes the 25$^{th}$ and 75$^{th}$ percentiles,

median, and data points not considered outliers. Those considered outliers are marked with a red plus sign. The mean fraction is plotted for each dataset and is represented by a blue shaded diamond. Generally, PW fractions are low across most datasets. However, an increase in PW/PFW fractions was observed in datasets 1997d, 2004, 2007, and 2018. Given 1997d and 2004 contained only one data point each in this water mass, these datasets may be considered as outliers to the overall trend. From all observations, there appears to be no temporal pattern as to when these fractions increase.

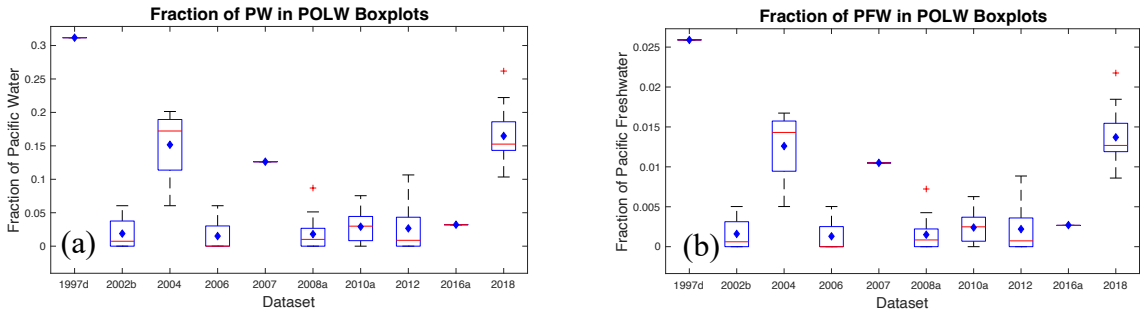


**Figure 19:** Box and whiskers time series plots for fractions of (a) PW and (b) PFW in the inner shelf section. Each box's bottom and top edges indicate the 25$^{th}$ and 75$^{th}$ percentiles, respectively. The median and mean are represented by the red horizontal line and blue shaded diamond, respectively. The whiskers extend to the data points not considered outliers and all outliers are plotted with the "+" symbol.

Few studies have analyzed PW/PFW fractions in this region of Greenland. The only study that did so utilized 2004 data and identified the PW fraction to be less than 0.10 (Sutherland et al., 2009). That finding is somewhat consistent with those presented here, as 2004's data within the POLW water mass has a mean PW fraction of 0.15. Although this fraction is slightly greater than the published value, this finding can be viewed as consistent, given how data was partitioned into POLW prior to analysis in this study. As there are no other studies that conducted analysis in this study's region, reviewing results from further upstream is the best alternative. Data from an area around 400 miles northeast of this study's region in the Denmark

Strait reveals the following fractions of PFW: small amount from 1991-1998, a significant increase in 1999, none from 2002-2004, 2011: 0.03, 2012: 0.04, and 2013: 0.05 (Sutherland et al., 2009 and de Steur et al., 2015). Due to the differences in study area and as expected, these published values differ from this study's findings, as this study's data observed relatively large PFW presences in 1997 and 2004 when compared to other years and much lower fractions of PFW in 2010 and 2012, surrounding years of published fractions. These findings indicate that large changes occur in PW/PFW fractions from one area upstream to another further downstream, as increased mixing of other freshwater sources (i.e. Greenland ice sheet run-off) further south results in a decrease of Pacific-origin water. Several studies have conducted analysis on the fractions of PW/PFW in western Fram Strait, but due to the notion above and as a result, the relevance to this study's area to calculated values that far north, these studies were not compared to this study's findings. In Table 6 below, PW and PFW mean fractions for all applicable datasets are listed by shelf section. These results further exemplify that there are no visible temporal trends associated with these fractions within the POLW water mass.

**Table 6:** Mean fractions of PW and PFW categorized by dataset. Fractions were only calculated for samples in water mass POLW and if the samples contained both nitrate and phosphate values. The number of observations of samples in POLW for each dataset is listed in parenthesis.

| **Dataset (inner)** | **PW** | **PFW** |
|---|---|---|
| 1997d (1) | 0.3117 | 0.0259 |
| 2002b (4) | 0.0188 | 0.0016 |
| 2004 (4) | 0.1516 | 0.0126 |
| 2006 (4) | 0.0151 | 0.0013 |
| 2007 (1) | 0.1263 | 0.0105 |
| 2008a (15) | 0.0180 | 0.0015 |
| 2010a (17) | 0.0291 | 0.0024 |
| 2012 (17) | 0.0266 | 0.0022 |
| 2016a (1) | 0.0321 | 0.0027 |
| 2018 (19) | 0.1648 | 0.0137 |

### 3.6 Nutrient-to-nutrient relationships

Reviewing relationships between nutrients and comparing these relationships to accepted literature values assists in identifying how each nutrient interacts with one another in the marine environment. With an accepted global relationship between C:Si:N:P of 106:15:16:1, the Redfield-Brzezinski ratio (Brzezinski 2004) is an important biogeochemical indicator and is used to identify nutrients that are diminished and possibly limiting life in the marine environment.

In Figures 20 and 21 below, Figures 20 (a), (b), and (c) are relationships between nitrate and phosphate, nitrate and silicate, and silicate and phosphate, respectively, within the inner shelf colored by dataset. Further below, Figures 21 (a), (b), and (c) are the same relationships, but for the outer shelf section. For context, each plot contains the 95% confidence intervals for those respective nutrients denoted with a blue box and labeled as such for context, indicating that there is a 95% probability that the true values for each respective water mass lie in those respective boxes. Additionally, a linear trend line is fitted to the data. Both the slope and intercept for this trend line are listed in each figure's respective legend. If relationships between each nutrient are similar to the accepted ratio, then the respective slopes for each of the three plots from left to right should be 16, 1.07, and 15, respectively. Although there are no previously published ratios in this region of study, waters close to the surface in southwest Greenland have ratios for N:P, N:Si, and Si:P of 6:1 – 9:1, 1:1 – 1.3:1, and 6:1-7:1, respectively (Tesdal et al., 2022). The southwestern area of Greenland experiences vastly different oceanographic forcings from this study's research area, so the ratios from that study are not expected to be similar to those in this study, but are still worth mentioning. Another detail to note in the nutrient-to-nutrient plots is the sign of the y intercept, as a negative intercept signifies that the x-axis nutrient diminishes quicker than the y-axis nutrient and vice versa. Finally, the last detail to note for each plot is the overall

trend of the data, as the last two plots for each grouping of shelf sections indicate a horizontal and vertical asymptote, respectively. This detail provides evidence as to which nutrient is more enriched when the other nutrient in the plot has leveled off in available concentrations.

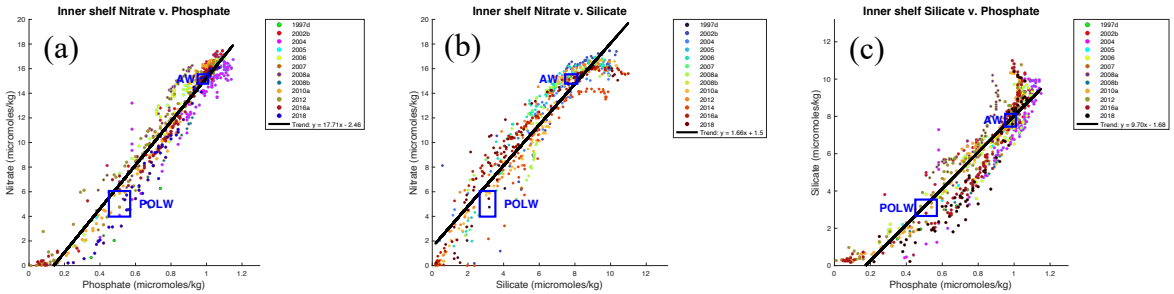


**Figure 20:** Inner shelf nutrient sample concentrations with datasets plotted by color. Above are plots for (a) nitrate versus phosphate, (b) nitrate versus silicate, and (c) silicate versus phosphate, respectively. The solid black line is a linear trend line for the data within each plot. The regression line's slope and intercept for each plot are found in each respective legend. The blue rectangles denote the respective 95% confidence intervals of the AW and POLW water masses, and are notated as such.

Analyzing the inner shelf section first, Figures 20 (a), (b), and (c) have linear slopes of 17.71, 1.66, and 9.70, with y-intercepts of -2.46, 1.5, and -1.68, respectively. The lower concentrations for both axes (lower left corner of each figure) are data from shallower waters and the higher concentrations for both axes (upper right corner of each figure) are data from a wider range of depths from sub-surface to bottom. Looking at how these relationships compare to the accepted values, only Figure 20 (a)'s slope compares favorably to the accepted N:P ratio of 16. The other two slopes are off by a significant margin from the N:Si and Si:P ratios of 1.07 and 15, respectively. These differences are likely due to the location of the observations, what physical (upwelling) and biological (increased productivity) forces are at play compared to open-ocean observations, and what microorganisms inhabit this study's waters. Additionally, if samples matched the accepted ratios, each figure would have an intercept of 0. However, this is not observed. Given Figures 20 (a) and (c) have negative y-intercepts and slight horizontal

asymptotes at shallower depths, it indicates that both y axes variables are not as available compared to the respective x axes variables, meaning both nitrate and silicate are utilized quicker and/or remineralized less than phosphate. At depth, Figure 20 (c) indicates that silicate is in higher concentration than phosphate, which concurs with the mean interpolated plots that exhibited increased silicate at depth when compared to the other nutrients. In review of Figure 20 (b), the linear trend line is likely not fit to the data points as best as it could be, as there is evidence of a horizontal asymptote at increased depth, which likely skews the intercept to be placed on the y axis. Therefore, it is more likely that nitrate is utilized more or remineralized at lower rates than silicate in this environment. This notion is also supported by the horizontal asymptote, in that at depth, silicate is more available than nitrate. From these observations of Figures 20 (a), (b), and (c), it is concluded that the nutrient that is utilized quickest and remains in short supply in the inner shelf section is nitrate, then silicate, then phosphate. These findings can also be associated with less remineralization of nitrate when compared to both silicate and phosphate. However, live samples of microorganisms in the area would be needed to conclude this.

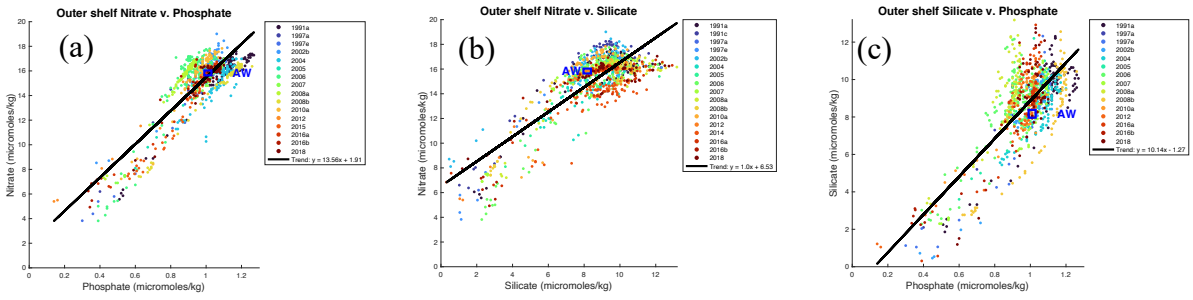


**Figure 21:** Outer shelf nutrient sample concentrations with datasets plotted by color. Above are plots for (a) nitrate versus phosphate, (b) nitrate versus silicate, and (c) silicate versus phosphate, respectively. The solid black line is a linear trend line for the data within each plot. The regression line's slope and intercept for each plot are found in each respective legend. The blue rectangle in each subfigure denotes the respective 95% confidence interval for the AW water mass.

In review of the outer shelf section's plots above, Figures 21 (a), (b), and (c) have linear slopes of 13.56, 1.0, and 10.14, with y-intercepts of 1.91, 6.53, and -1.27, respectively. Similar to the inner shelf section, the 95% confidence interval for both nutrients being compared within each plot is identified by a blue box. Also similar, the lower left corners of each figure display data from shallower depths and the upper right corners of each figure include data at deeper depths. In these plots, it is evident that there are much fewer data points at shallower depths when compared to deep depths, which is to be expected in this section. A comparison of each of the figure's slopes to the Redfield-Brzezinski ratios indicate that both N:Si and Si:P exhibit a closer relation to the global ratios, while N:P exhibits a relationship not as close when compared to the inner shelf section ratios. Also of note, the only ratio that was similar to the southwestern Greenland values came from this shelf's nitrate versus silicate plot, noting that relationships between nutrients are vastly different between the two coasts of southern Greenland. Additionally, the respective asymptotes in the nitrate versus silicate and silicate versus phosphate plots remain present, which indicates similar relationships exhibited at depth as before where silicate was expected to remineralize more than both nitrate and phosphate. From these observations of Figures 21 (a), (b), and (c), it is concluded that both nitrate and phosphate are co-limiting or remineralized at similar rates, while silicate is the most plentiful of the three nutrients within the outer shelf section. This evidence supports the notion stated by Moore et al. (2013) previously cited in this study, that the North Atlantic nearby the region of this study is limited by nitrate, then phosphate, and then, silicate.

### 3.7 Errors and Uncertainties

Potential sources of error and uncertainty within this investigation are introduced via the methods chosen in data collection and processing, the samples themselves, and in calculation of

the results. First, when gridding data from in-situ observations of hydrographic and nutrient measurements used in interpolation, casts lying outside of specific boundaries from the gridded points (10 km for the inner shelf and 30 km for the outer shelf) were removed. These distances were carefully selected based on the rate of change to bathymetry over the observed areas and the locations of available data. However, in review of several difference from mean plots both for CTD and nutrient data, a more selective approach by narrowing boundaries to remove casts may have ensured more continuity between datasets at specific locations. However, this method would have limited the number of casts used in interpolation, which would not have been as representative to true data as present interpolation methods. It is also possible that the apparent differences deemed potential errors within these plots could have been a product of the datasets themselves. Given observations were sampled by multiple scientists over a period of nearly three decades, oftentimes without standardization of recording procedures or instrumentation used in measurements between them, it is possible that differences between datasets were possible and even, likely. Large differences observed within the difference from mean plots may have been caused by these potential errors.

Another possible source of error may exist within sample concentrations due to biologic uptake, as concentrations are linked to changes in primary production within the photic zone. Nutrient quantities change drastically during phytoplankton blooms, mainly in near-surface waters, so if a particular year exhibited a much later bloom of marine primary producers than the April average, this may have influenced quantities enough to constitute a difference in near-surface waters. Also associated with biologic uptake, an inherent ±10% uncertainty was factored into PW and PFW calculations during previous studies, as potential denitrification or nitrogen fixation within the Arctic and along the Greenland continental shelf is likely to affect the

measured relationship between nitrate and phosphate. This degree of uncertainty was factored into this study's calculations as well. Finally, additional errors may exist within these calculations, as the AW source line used here was taken from Dodd et al. (2012) and was characteristic of AW entering the Arctic Ocean, rather than waters that had been circulated via the IC along southeastern Greenland. Although both waters have similar pathways and are fed by the NAC, calculations may differ slightly from true Atlantic source water in this region.

# CHAPTER 4: CONCLUSION

## 4.1 Conclusions

From in-situ observations between 2002 and 2016, the first result of this study is that the mean nutrient distributions on the southeast Greenland continental shelf and slope were largely linked to freshwater flux, transport of both surface and deep-water currents, and open-ocean water masses in the North Atlantic subpolar gyre. Nutrients were in lowest concentrations at the surface and furthest inshore. Coupled with the presence of cold and fresh water in the same area, this likely indicates the presence of either Greenland ice sheet meltwater or polar-origin water transported by both the EGCC and EGC. These waters have lower nutrient composition than those further off shore and at depth. The intrusion of AW was observed further inshore at depth compared to the surface, which indicates the influence of EGC transport, particularly closer to the surface. Further conclusions linking the EGC and EGCC to nutrient transport cannot be made without water velocity measurements. Within the inner shelf section from inshore to offshore and surface to bottom, nutrient concentrations increased. Beyond the continental shelf and further offshore, nutrients increased much more rapidly with depth, potentially indicating the utilization of these nutrients by primary producers within the euphotic zone, which was an expected result. Nutrients exhibited a maximum further offshore and at depth, shallowest for nitrate, deeper for phosphate, and deepest for silicate, indicating that nutrients are depleted in this order within the region. Interpolating nutrients using measurements closest to the gridded points in this study yielded no apparent signal associated with interannual variability between years.

The second result of this investigation is that AW had two to three times greater nutrients than POLW. This is consistent with previous studies and is most likely due to the entrainment of nutrients in open-ocean water masses. For the inner shelf section, AW nitrate, phosphate, and

silicate concentrations (measured in μmol/kg) at the 95% confidence interval were (14.78, 15.54), (0.95, 1.01), and (7.45, 8.15), respectively. The same confidence intervals for the outer shelf AW were similar to the above at (15.64, 16.04), (0.99, 1.03), and (7.96, 8.38), respectively. Finally, for POLW, these confidence intervals decreased significantly, with concentrations of nitrate, phosphate, and silicate at (3.98, 6.06), (0.45, 0.57), and (2.66, 3.54), respectively. AW exhibited greater variability between years, but because there were more datasets that sampled this water mass, the 95% confidence intervals were tighter than those exhibited by POLW. Phosphate concentrations demonstrate more temporal variability than both nitrate and silicate, which is likely due to the small concentrations of this nutrient in the marine environment and the effect on measurements. Atlantic-origin water masses including IrSPMW, LSW, and ISOW were observed further offshore and at-depth, each with their own nutrient compositions, which were similar to published values. Water mass nutrient concentrations for AW and POLW often varied between this study and others. This is likely due to both the difference in locations to previous studies and the definitions of water masses found in this study compared to others. These results were expected, as oceanographic forcings and influences vary greatly between Fram Strait and southeastern Greenland.

The third result is that using sample concentrations found closest to the gridded points in this study yielded no obvious signal of interannual variability for mean fractions of PW and PFW in the POLW water mass. Due to the distance between Fram Strait and this study, lower fractions of both PW and PFW were expected and measured. Excluding datasets with only one POLW sample, an increase in Pacific-origin waters was shown in 2004 and 2018. Mean fractions of PW and PFW in 2004 were 0.15 and 0.01, respectively, while the same respective fractions in 2018 were 0.16 and 0.01. This result was similar to a previous study of an individual year for 2004

only. No other studies were found for this area and timeframe, so results were compared to those from the Denmark Strait, which expectedly differed from this study's results due to the differences between the two sampling regions. Sources of freshwater in this region are mostly not of Pacific-origin and are instead, likely remnants of Greenland ice sheet mass loss or sea ice transport through western Fram Strait.

The final result is that the relationships between nutrients for both the inner and outer shelf sections indicate that nitrate was potentially the most limiting nutrient, followed closely behind by phosphate, and then, silicate. This could indicate that nitrate was either the nutrient that was utilized the most or remineralized the least compared to the other two. This finding concurs with previous results of the mean nutrient concentrations, which indicated that at depth and further offshore, nitrate reached a maximum at the shallowest depth, followed closely behind by phosphate, and then, silicate. This order of limiting nutrients also concurs with previous studies in the North Atlantic region. From relationships observed between nutrients, ratios of N:P, N:Si, and Si:P were deduced in both shelf sections from the calculated slope when nutrients were plotted against one another. The inner shelf exhibited ratios of 17.71, 1.66, and 9.70, respectively, while the outer shelf displayed ratios of 13.56, 1.00, and 10.14, respectively. As expected and similar to previous literary sources, these ratios differed slightly from the accepted Redfield-Brzezinski ratios of 16, 1.07, and 15, respectively. Based on these differences, ratios calculated here exhibited characteristics of both polar and upwelling regions, which is consistent with the location of this study.

### 4.2 Future Studies

A logical progression of this research would be a comprehensive investigation into the relationship between the strength of the Arctic Oscillation (AO) index and PW fractions in

southeastern Greenland. The AO is a mode of climate variability exhibited in the northern latitudes that is linked to the strength of the Beaufort Gyre in the Arctic Ocean (Sutherland et al., 2009). Previous studies have determined a correlation between the phase of the AO and PW pathways, meaning that a positive AO phase weakens the Beaufort Gyre and allows more PW to pass through Fram Strait (Steele et al., 2004). Sutherland et al. (2009) identified a correlation between the two, but only observed data from the Denmark Strait. Data from this study's research area could be utilized to facilitate a comparison. Another next step could be to link fractions of PW to the possible interannual variability of the EGC/EGCC system in southeastern Greenland using current velocity measurements within the area. It is unclear if these measurements exist for this time period and area, but perhaps this could be a reasonable topic of interest. Finally, if available throughout the years of this study, oxygen isotope (delta $^{18}O$) and alkalinity measurements could be extracted from databases and utilized to calculate fractions of sea ice meltwater and meteoric water in order to assess additional sources of freshwater input to southeastern Greenland besides those measured in this study.

APPENDIX A

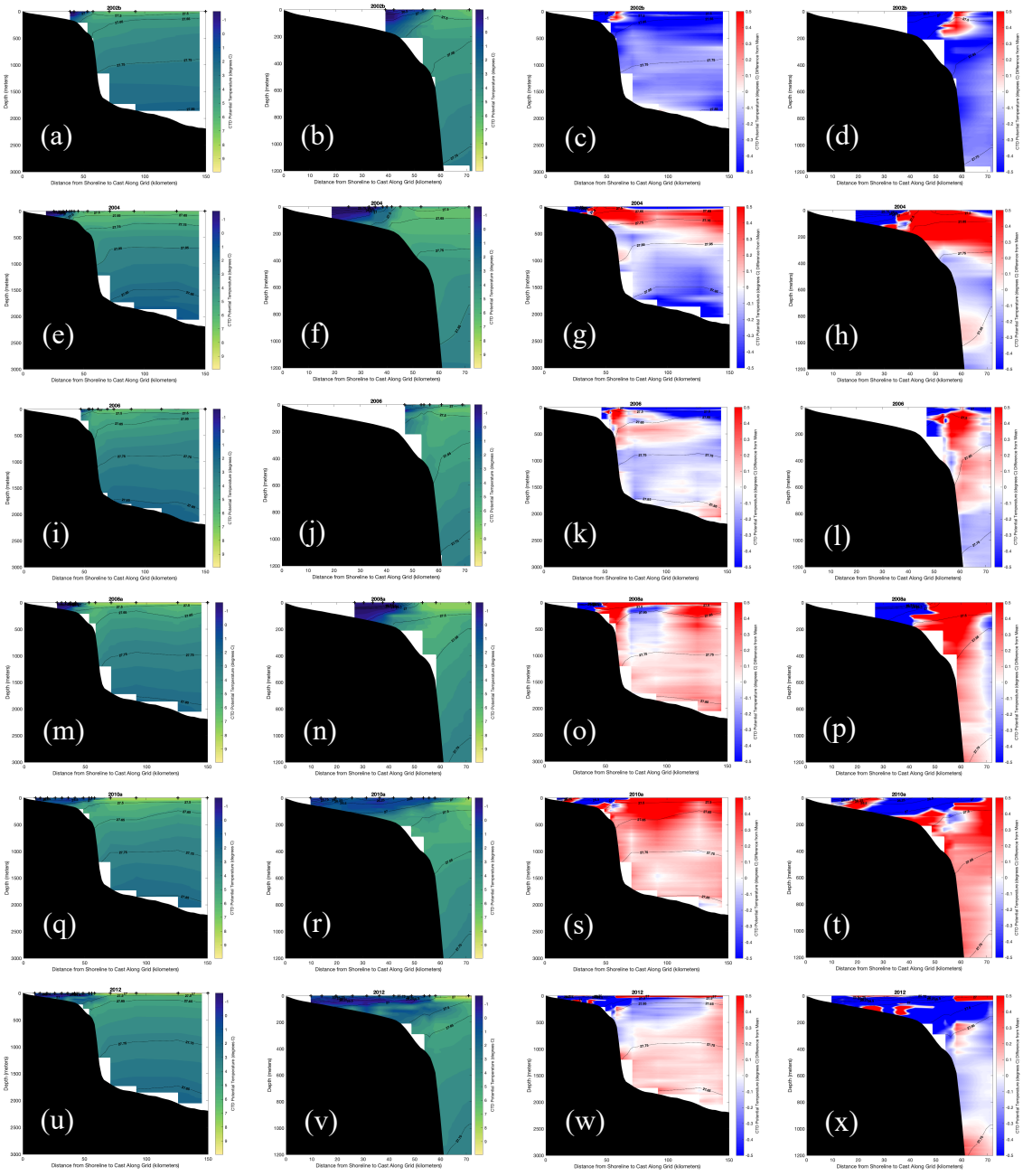


**Figure 22:** For each row from left to right, CTD potential temperatures (green) for both shelves and inner shelf, and difference from mean CTD potential temperature (red and blue) for both shelves and inner shelf, for (a-d) 2002b, (e-h) 2004, (i-l) 2006, (m-p) 2008, (q-t) 2010a, (u-x) 2012, (y-bb) 2014, (cc-ff) 2016a, respectively. The black "+" signs in the CTD temperature plots denote the locations of each cast in distance along the grid. The solid black lines denote isopycnals in kg/m$^3$.

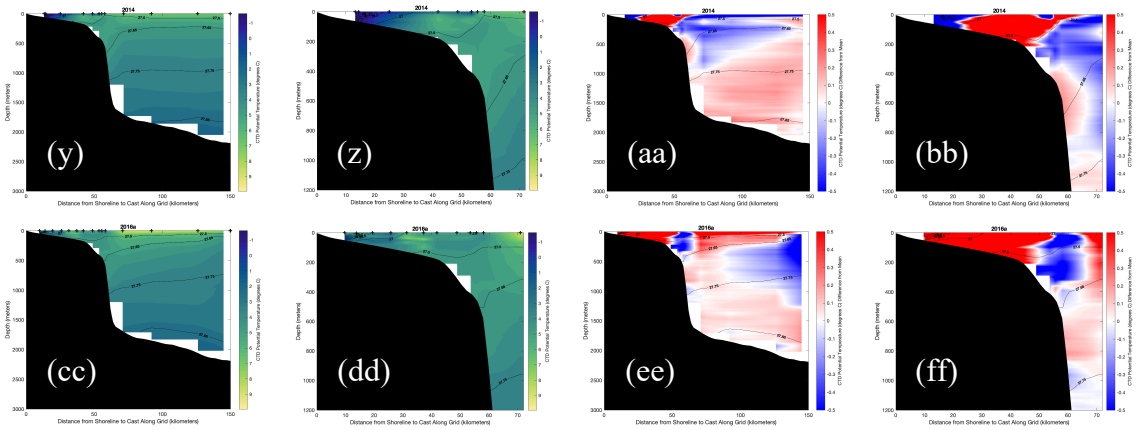


**Figure 22, Continued:** For each row from left to right, CTD potential temperatures (green) for both shelves and inner shelf, and difference from mean CTD potential temperature (red and blue) for both shelves and inner shelf, for (a-d) 2002b, (e-h) 2004, (i-l) 2006, (m-p) 2008, (q-t) 2010a, (u-x) 2012, (y-bb) 2014, and (cc-ff) 2016a, respectively. The black "+" signs in the CTD temperature plots denote the locations of each cast in distance along the grid. The solid black lines denote isopycnals in kg/m$^3$.

APPENDIX B

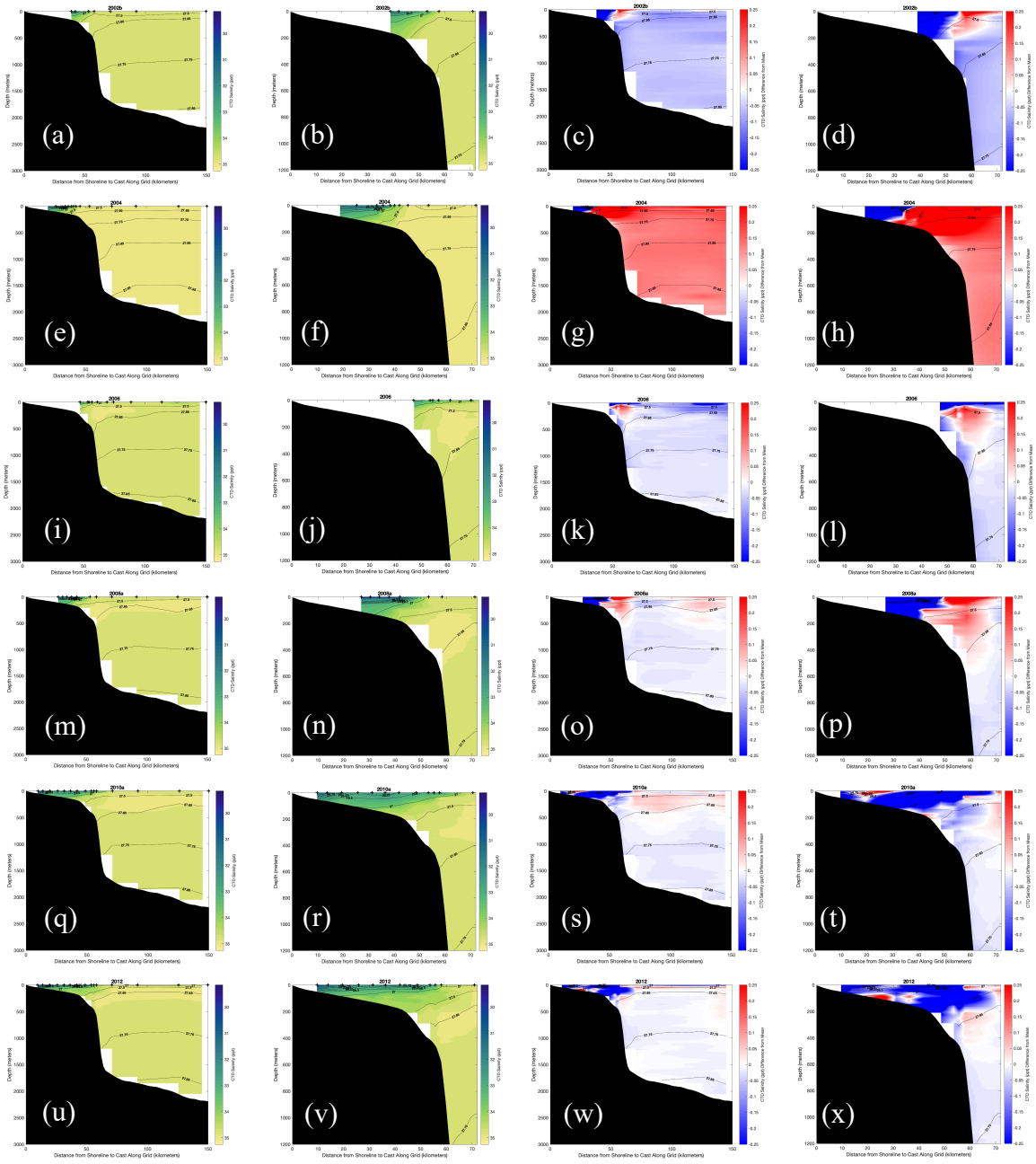


**Figure 23:** For each row from left to right, CTD salinity (green) for both shelves and inner shelf, and difference from mean CTD salinity (red and blue) for both shelves and inner shelf, for (a-d) 2002b, (e-h) 2004, (i-l) 2006, (m-p) 2008, (q-t) 2010a, (u-x) 2012, (y-bb) 2014, and (cc-ff) 2016a, respectively. The black "+" signs in the CTD salinity plots denote the locations of each cast in distance along the grid. The solid black lines denote isopycnals in kg/m$^3$.

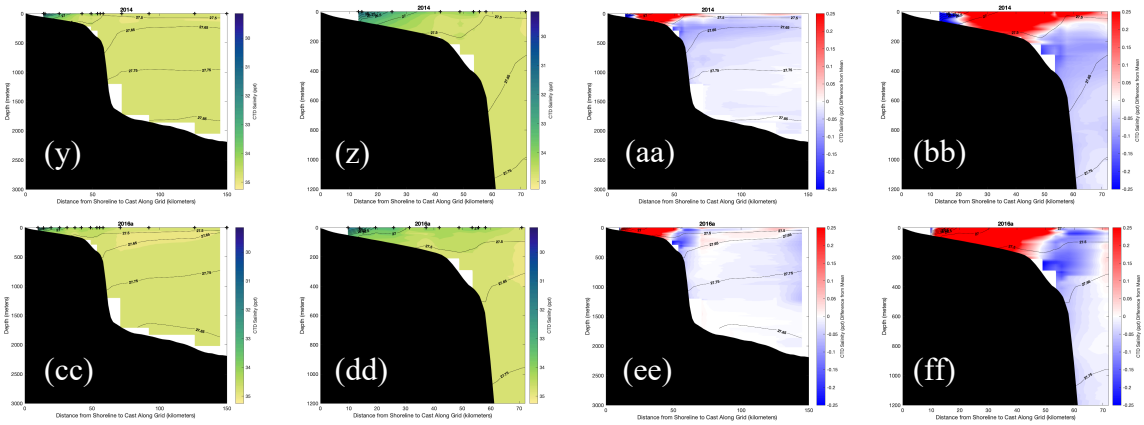


**Figure 23, Continued:** For each row from left to right, CTD salinity (green) for both shelves and inner shelf, and difference from mean CTD salinity (red and blue) for both shelves and inner shelf, for (a-d) 2002b, (e-h) 2004, (i-l) 2006, (m-p) 2008, (q-t) 2010a, (u-x) 2012, (y-bb) 2014, and (cc-ff) 2016a, respectively. The black "+" signs in the CTD salinity plots denote the locations of each cast in distance along the grid. The solid black lines denote isopycnals in $kg/m^3$.

APPENDIX C

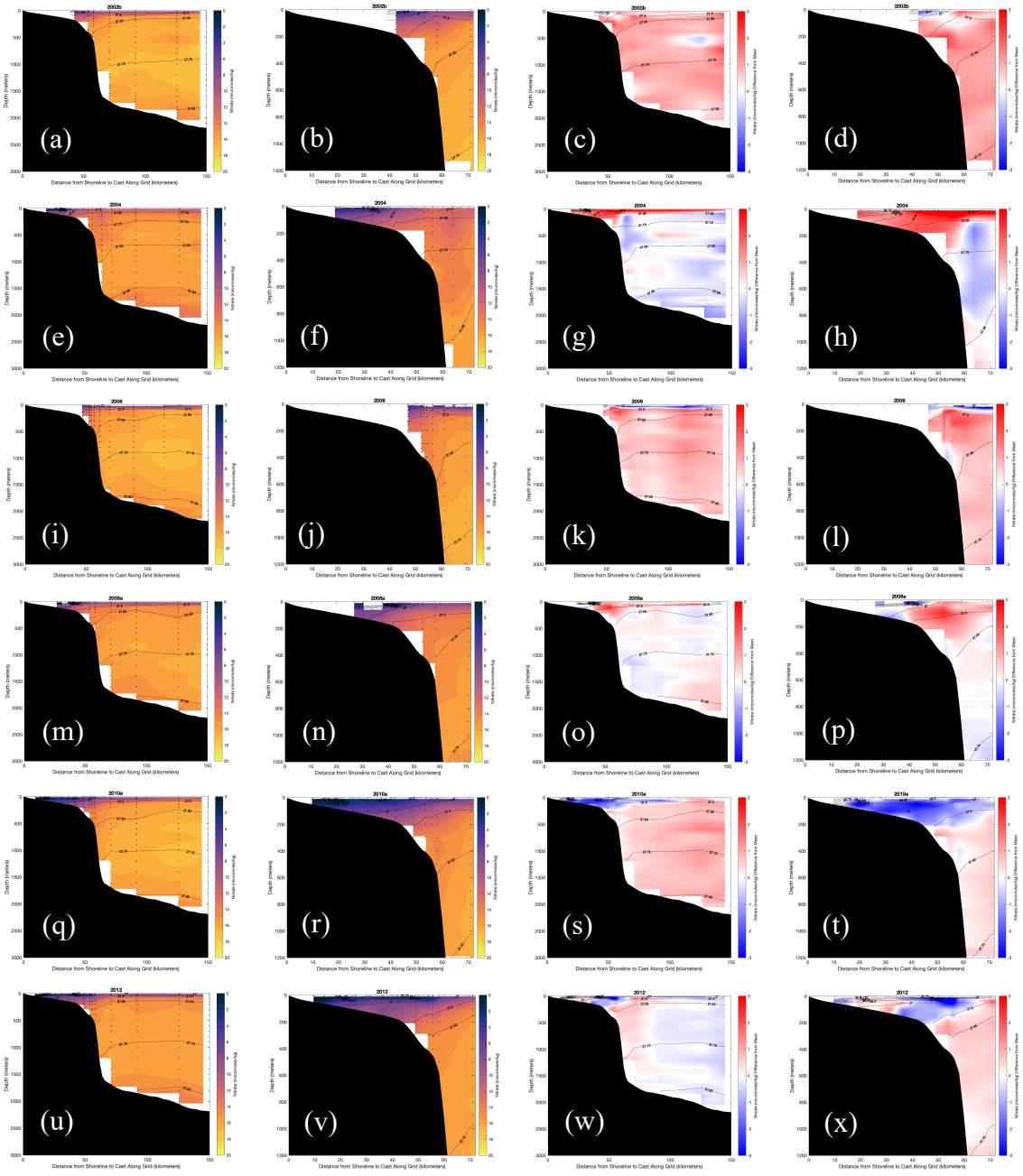


**Figure 24:** For each row from left to right, nitrate (orange) for both shelves and inner shelf, and difference from mean nitrate (red and blue) for both shelves and inner shelf, for (a-d) 2002b, (e-h) 2004, (i-l) 2006, (m-p) 2008, (q-t) 2010a, (u-x) 2012, (y-bb) 2014, and (cc-ff) 2016a, respectively. The black dots in the nitrate plots denote the locations and depths of each sample collected within the distance-depth grid. The solid black lines denote isopycnals in kg/m$^3$.

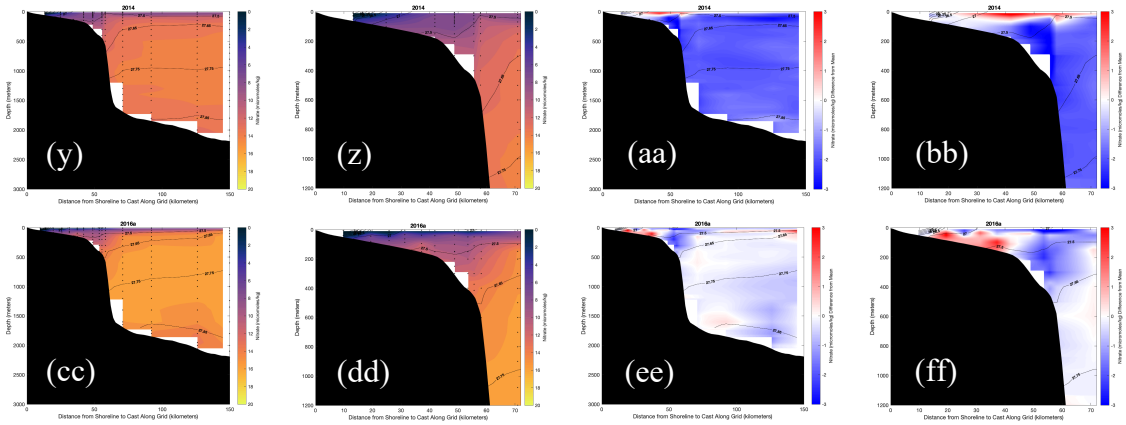


**Figure 24, Continued:** For each row from left to right, nitrate (orange) for both shelves and inner shelf, and difference from mean nitrate (red and blue) for both shelves and inner shelf, for (a-d) 2002b, (e-h) 2004, (i-l) 2006, (m-p) 2008, (q-t) 2010a, (u-x) 2012, (y-bb) 2014, and (cc-ff) 2016a, respectively. The black dots in the nitrate plots denote the locations and depths of each sample collected within the distance-depth grid. The solid black lines denote isopycnals in $kg/m^3$.

APPENDIX D

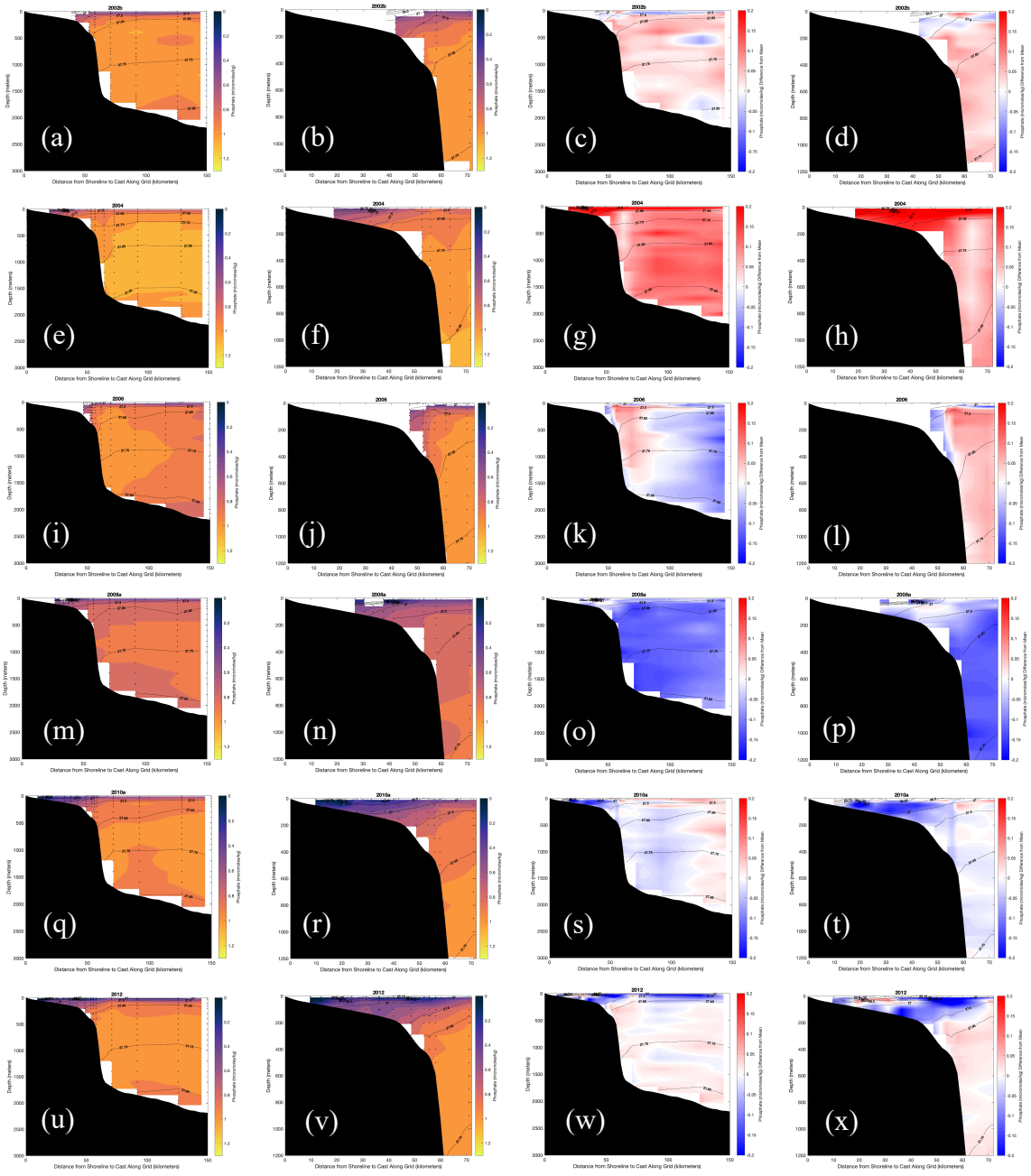


**Figure 25:** For each row from left to right, phosphate (orange) for both shelves and inner shelf, and difference from mean phosphate (red and blue) for both shelves and inner shelf, for (a-d) 2002b, (e-h) 2004, (i-l) 2006, (m-p) 2008, (q-t) 2010a, (u-x) 2012, (y-bb) 2014, and (cc-ff) 2016a, respectively. The black dots in the phosphate plots denote the locations and depths of each sample collected within the distance-depth grid. The solid black lines denote isopycnals in $kg/m^3$.

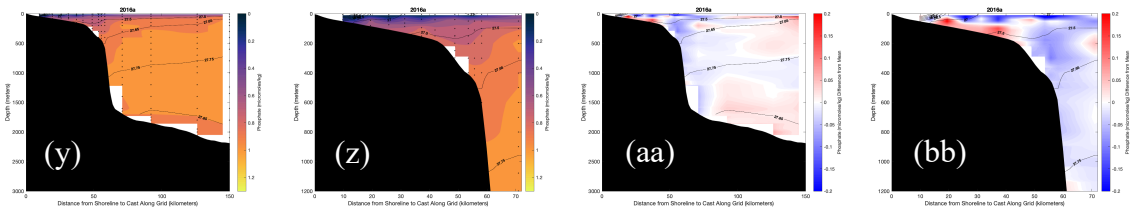


**Figure 25, Continued:** For each row from left to right, phosphate (orange) for both shelves and inner shelf, and difference from mean phosphate (red and blue) for both shelves and inner shelf, for (a-d) 2002b, (e-h) 2004, (i-l) 2006, (m-p) 2008, (q-t) 2010a, (u-x) 2012, and (y-bb) 2016a, respectively. The black dots in the phosphate plots denote the locations and depths of each sample collected within the distance-depth grid. The solid black lines denote isopycnals in $kg/m^3$.

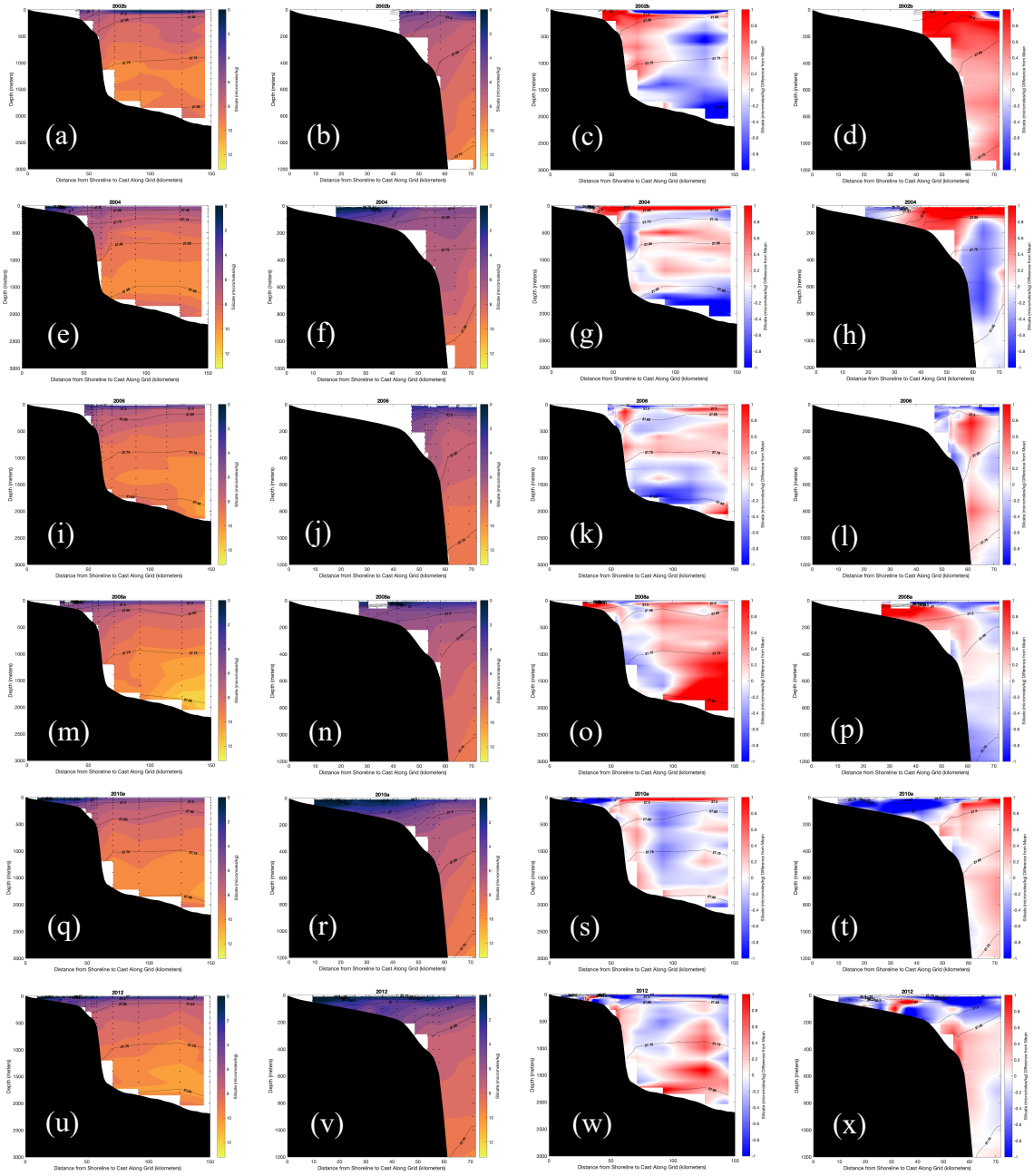


**Figure 26:** For each row from left to right, silicate (orange) for both shelves and inner shelf, and difference from mean silicate (red and blue) for both shelves and inner shelf, for (a-d) 2002b, (e-h) 2004, (i-l) 2006, (m-p) 2008, (q-t) 2010a, (u-x) 2012, (y-bb) 2014, and (cc-ff) 2016a, respectively. The black dots in the silicate plots denote the locations and depths of each sample collected within the distance-depth grid. The solid black lines denote isopycnals in kg/m$^3$.

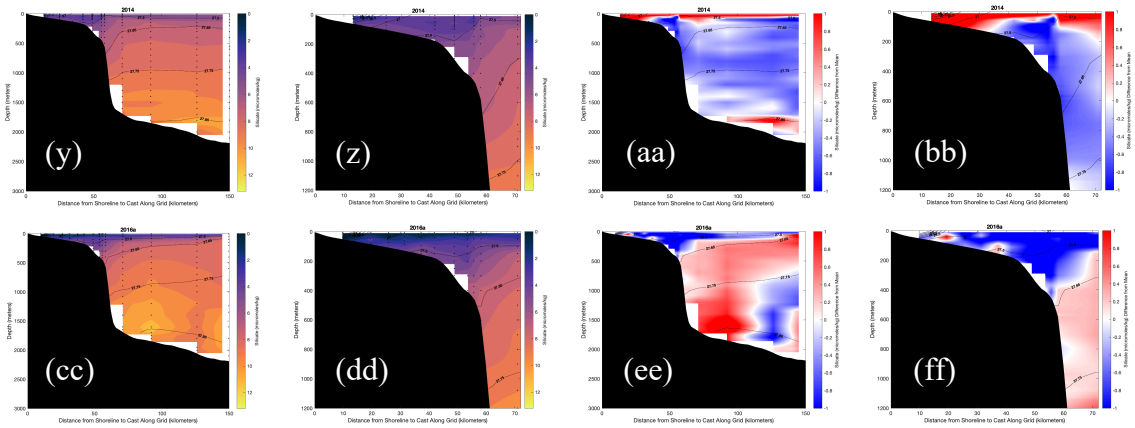


**Figure 26, Continued:** For each row from left to right, silicate (orange) for both shelves and inner shelf, and difference from mean silicate (red and blue) for both shelves and inner shelf, for (a-d) 2002b, (e-h) 2004, (i-l) 2006, (m-p) 2008, (q-t) 2010a, (u-x) 2012, (y-bb) 2014, and (cc-ff) 2016a, respectively. The black dots in the silicate plots denote the locations and depths of each sample collected within the distance-depth grid. The solid black lines denote isopycnals in $kg/m^3$.

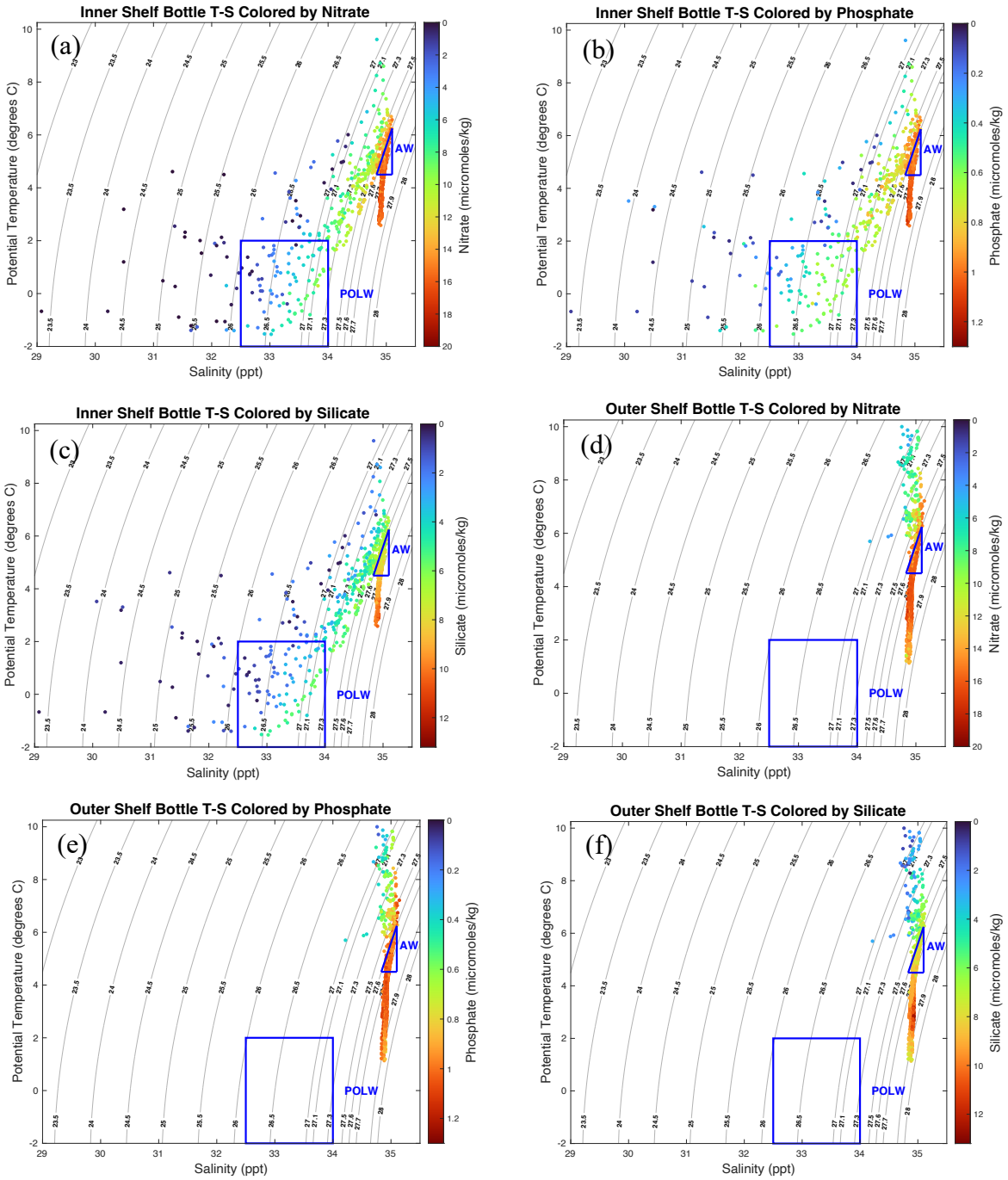


**Figure 27:** Potential temperature versus salinity for the inner shelf (a – c) and outer shelf (d – f) colored by nitrate (a, d), phosphate (b, e), and silicate (c, f), respectively. The solid black lines denote mean isopycnals in kg/m$^3$. The scales on both axes are the same for all plots, selected for maximum visibility of all data points. The blue triangle and rectangle denote the AW and POLW water masses, respectively.

REFERENCES


Armbrust, E. Virginia. “The Life of Diatoms in the World's Oceans.” *Nature*, vol. 459, no. 7244, 13 May 2009, pp. 185–192., https://doi.org/10.1038/nature08057. Accessed 5 Mar. 2023.

Auton, Adam. “Red Blue Colormap.” *MathWorks*, 2023, https://www.mathworks.com/matlabcentral/fileexchange/25536-red-blue-colormap.

Bacon, S. 2022. Bottle and CTD data from cruise 74DI20080820, WHP netCDF version. Accessed from CCHDO https://cchdo.ucsd.edu/cruise/74DI20080820. Access date 2022 09-07.

Bacon, S. 2022. Bottle data from cruise 74DI230_1, WHP netCDF version. Accessed from CCHDO https://cchdo.ucsd.edu/cruise/74DI230_1. Access date 2022-09-04. CCHDO cruise DOI 10.1029/2003JC002015.

Bamber, J., van den Broeke, M., Ettema, J., Lenaerts, J., and Rignot, E. “Recent Large Increases in Freshwater Fluxes from Greenland into the North Atlantic.” *Geophysical Research Letters*, vol. 39, no. 19, 16 Oct. 2012, https://doi.org/10.1029/2012gl052552. Accessed 20 Apr. 2023.

Beaton, A. D., Wadham, J. L., Hawkings, J., Bagshaw, E. A., Lamarche-Gagnon, G., Mowlem, M. C., and Tranter, M. “High-Resolution in Situ Measurement of Nitrate in Runoff from the Greenland Ice Sheet.” *Environmental Science & Technology*, vol. 51, no. 21, 27 Sept. 2017, pp. 12518–12527., https://doi.org/10.1021/acs.est.7b03121. Accessed 7 Dec. 2022.

Benitez-Nelson, Claudia R. “The Biogeochemical Cycling of Phosphorus in Marine Systems.” *Earth-Science Reviews*, vol. 51, no. 1-4, Aug. 2000, pp. 109–135., https://doi.org/10.1016/s0012-8252(00)00018-0. Accessed 10 Apr. 2023.

Bergman, B., Sandh, G., Lin, S., Larsson, J. and Carpenter, E. J. “Trichodesmium – a Widespread Marine Cyanobacterium with Unusual Nitrogen Fixation Properties.” *FEMS Microbiology Reviews*, vol. 37, no. 3, May 2013, pp. 286–302., https://doi.org/10.1111/j.1574-6976.2012.00352.x. Accessed 8 Dec. 2022.

Biology Dictionary. “Phosphate Group - Definition and Functions.” *Biology Dictionary*, 29 Apr. 2017, https://biologydictionary.net/phosphate-group/.

Brummer, G. 2022. Bottle and CTD data from cruise 64PE20070830, WHP netCDF version. Accessed from CCHDO https://cchdo.ucsd.edu/cruise/64PE20070830. Access date 2022 09-07.

Brzezinski, Mark A. “The Si:C:N Ratio of Marine Diatoms: Interspecific Variability and the Effect of Some Environmental Variables.” *Journal of Phycology*, vol. 21, no. 3, 29 Oct. 2004, pp. 347–357., https://doi.org/10.1111/j.0022-3646.1985.00347.x. Accessed 16 Nov. 2022.

Buckley, Martha W., and John Marshall. “Observations, Inferences, and Mechanisms of the Atlantic Meridional Overturning Circulation: A Review.” *Reviews of Geophysics*, vol. 54, no. 1, 22 Dec. 2015, pp. 5–63., https://doi.org/10.1002/2015rg000493. Accessed 3 Nov. 2022.

Cape, M. R., Straneo, F., Beaird, N., Bundy, R. M., and Charette, M. A., “Nutrient Release to Oceans from Buoyancy-Driven Upwelling at Greenland Tidewater Glaciers.” *Nature Geoscience*, vol. 12, no. 1, Jan. 2019, pp. 34–39., https://doi.org/10.1038/s41561-018-0268-4. Accessed 4 Feb. 2023.

Capone, D. G., Zehr, J. P., Paerl, H. W., Bergman, B., and Carpenter, E. J. “Trichodesmium, a Globally Significant Marine Cyanobacterium.” *Science*, vol. 276, no. 5316, 23 May 1997, pp. 1221–1229., https://doi.org/10.1126/science.276.5316.1221. Accessed 2 Dec. 2022.

Comiso, J. C., Parkinson, C. L., Gersten, R., and Stock, L. “Accelerated Decline in the Arctic Sea Ice Cover.” *Geophysical Research Letters*, vol. 35, no. 1, 3 Jan. 2008, https://doi.org/10.1029/2007gl031972. Accessed 15 Oct. 2022.

Demirel, Yaşar, and Vincent Gerbaud, editors. “Chapter 11: Thermodynamics and Biological Systems.” *Nonequilibrium Thermodynamics Transport and Rate Processes in Physical and Biological Systems*, 4th ed., Elsevier, Amsterdam, 2019, pp. 501–502, https://reader.elsevier.com/reader/sd/pii/B9780444641120000113?token=7650B165A75E75BA1A999C5AF241FCCA4F1734F21E46D68998F8FCD35DC1AA81AFBEDE58B5E025AB635C3C96C9FB9A6A&originRegion=us-east-1&originCreation=20230411210059. Accessed 11 Apr. 2023.

de Jong, M. & de Steur, L. (2019). Cruise 64PE400: Hydrographic survey of the Irminger Sea in July 2015 for the Overturning in the Subpolar North Atlantic Program (OSNAP). Bottle and CTD Data. SEANOE. https://doi.org/10.17882/59302

de Steur, L., Hansen, E., Gerdes, R., Karcher, M., Fahrbach, E., and Holfort, J. “Freshwater Fluxes in the East Greenland Current: A Decade of Observations.” *Geophysical Research Letters*, vol. 36, no. 23, Dec. 2009, https://doi.org/10.1029/2009gl041278. Accessed 20 Apr. 2023.

de Steur, L., Pickart, R. S., Macrander, A., Våge, K., Harden, B., Jónsson, S., Østerhus, S., and Valdimarsson, H. “Liquid Freshwater Transport Estimates from the East Greenland Current Based on Continuous Measurements North of Denmark Strait.” *Journal of Geophysical Research: Oceans*, vol. 122, no. 1, Jan. 2017, pp. 93–109., https://doi.org/10.1002/2016jc012106. Accessed 20 Apr. 2023.

de Steur, L., Pickart, R. S., Torres, D. J., and Valdimarsson, H. “Recent Changes in the Freshwater Composition East of Greenland.” *Geophysical Research Letters*, vol. 42, no. 7, 10 Mar. 2015, pp. 2326–2332., https://doi.org/10.1002/2014gl062759. Accessed 1 Feb. 2023.

Dickson, R., Rudels, B. Dye, S. Karcher, M. Meincke, J., and Yashayaev, I. "Current Estimates of Freshwater Flux through Arctic and Subarctic Seas." *Progress in Oceanography*, vol. 73, no. 3-4, 2007, pp. 210–230., https://doi.org/10.1016/j.pocean.2006.12.003.

Dipper, Frances. "1.3.2 Pelagic Deposits." *Elements of Marine Ecology*, 5th ed., Butterworth-Heinemann, an Imprint of Elsevier, Amsterdam, 2022, https://www.sciencedirect.com/science/article/pii/B9780081028261000119. Accessed 12 June 2023.

Dodd, P. A., Rabe, B., Hansen, E., Falck, E., Mackensen, A., Rohling, E., Stedmon, C., and Kristiansen, S. "The Freshwater Composition of the Fram Strait Outflow Derived from a Decade of Tracer Measurements." *Journal of Geophysical Research: Oceans*, vol. 117, no. C11, 6 Nov. 2012, https://doi.org/10.1029/2012jc008011. Accessed 17 Mar. 2023.

Duarte, P., Meyer, A., and Moreau, S. "Nutrients in Water Masses in the Atlantic Sector of the Arctic Ocean: Temporal Trends, Mixing and Links with Primary Production." *Journal of Geophysical Research: Oceans*, vol. 126, no. 8, 22 July 2021, https://doi.org/10.1029/2021jc017413. Accessed 4 Feb. 2023.

Durak, G. M., Taylor, A. R., Walker, C. E., Probert, I., de Vargas, C., Audic, S., Schroeder, D., Brownlee, C., and Wheeler, G. L. "A Role for Diatom-like Silicon Transporters in Calcifying Coccolithophores." *Nature Communications*, vol. 7, no. 1, 4 Feb. 2016, https://doi.org/10.1038/ncomms10543. Accessed 7 Mar. 2023.

Dukhovskoy, D. S., Yashayaev, I., Proshutinsky, A. Bamber, J. L., Bashmachnikov, I. L., Chassignet, E. P., Lee, C. M., and Tedstone, A. J. "Role of Greenland Freshwater Anomaly in the Recent Freshening of the Subpolar North Atlantic." *Journal of Geophysical Research: Oceans*, vol. 124, no. 5, May 2019, pp. 3333–3360., https://doi.org/10.1029/2018jc014686. Accessed 13 Oct. 2023.

García-Ibáñez, M. I., Pardo, P. C., Carracedo, L. I., Mercier, H., Lherminier, P., Ríos, A. F., and Pérez, F. F. "Structure, Transports and Transformations of the Water Masses in the Atlantic Subpolar Gyre." *Progress in Oceanography*, vol. 135, 2015, pp. 18–36., https://doi.org/10.1016/j.pocean.2015.03.009. Accessed 9 Feb. 2023.

Garrison, Tom. *Oceanography: An Invitation to Marine Science*. Brooks/Cole, 2010.

Gould, W. 2022. Bottle data from cruise RRS Charles Darwin Cruise 62, WHP netCDF version. Accessed from BODC. Access date 2022-09-11.*

Hawkings, J., Wadham, J., Tranter, M., Telling, J., Bagshaw, E., Beaton, A., Simmons, S., Chandler, D., Tedstone, A., and Nienow, P. "The Greenland Ice Sheet as a Hot Spot of Phosphorus Weathering and Export in the Arctic." *Global Biogeochemical Cycles*, vol. 30, no. 2, 13 Jan. 2016, pp. 191–210., https://doi.org/10.1002/2015gb005237. Accessed 9 Dec. 2022.

Hawkings, J. R., Wadham, J. L., Benning, L. G., Hendry, K. R., Tranter, M., Tedstone, A., Nienow, P., and Raiswell, R. "Ice Sheets as a Missing Source of Silica to the Polar Oceans." *Nature Communications*, vol. 8, no. 1, 25 Jan. 2017, https://doi.org/10.1038/ncomms14198. Accessed 2 Mar. 2023.

Holliday, N. P., Bersch, M., Berx, B., Chafik, L., Cunningham, S., Florindo- López, C., Hátún, H., Johns, W., Josey, S. A., Larsen, K. M., Mulet, S., Oltmanns, M., Reverdin, G., Rossby, T., Thierry, V., Valdimarsson, H., and Yashayaev, I. "Ocean Circulation Causes the Largest Freshening Event for 120 Years in Eastern Subpolar North Atlantic." *Nature Communications*, vol. 11, no. 1, 29 Jan. 2020, https://doi.org/10.1038/s41467-020-14474-y. Accessed 8 Mar. 2023.

Hopwood, M. J., Carroll, D., Browning, T. J., Meire, L., Mortensen, J., Krisch, S., and Achterberg, E. P. "Non-Linear Response of Summertime Marine Productivity to Increased Meltwater Discharge around Greenland." *Nature Communications*, vol. 9, no. 1, 14 Aug. 2018, https://doi.org/10.1038/s41467-018-05488-8. Accessed 4 Feb. 2023.

Huck, T. 2022. Bottle and CTD data from cruise 35TH20040604, WHP netCDF version. Accessed from CCHDO https://cchdo.ucsd.edu/cruise/35TH20040604. Access date 2022-08-28.

Huck, T. and Mercier, H. 2022. Bottle and CTD data from cruise 35TH20100610, WHP netCDF version. Accessed from CCHDO https://cchdo.ucsd.edu/cruise/35TH20100610. Access date 2022-08-28.

Johnson, C., Inall, M., and Häkkinen, S. "Declining Nutrient Concentrations in the Northeast Atlantic as a Result of a Weakening Subpolar Gyre." *Deep Sea Research Part I: Oceanographic Research Papers*, vol. 82, Dec. 2013, pp. 95–107., https://doi.org/10.1016/j.dsr.2013.08.007. Accessed 14 Apr. 2023.

Jones, E. M., Chierici, M., Menze, S., Fransson, A., Ingvaldsen, R. B., and Lødemel, H. H. "Ocean Acidification State Variability of the Atlantic Arctic Ocean around Northern Svalbard." *Progress in Oceanography*, vol. 199, Dec. 2021, https://doi.org/10.1016/j.pocean.2021.102708. Accessed 19 Jan. 2023.

Jones, E. P., Anderson, L. G., Jutterström, S., Mintrop, L., and Swift, J. H. "Pacific Freshwater, River Water and Sea Ice Meltwater across Arctic Ocean Basins: Results from the 2005 Beringia Expedition." *Journal of Geophysical Research*, vol. 113, no. C8, 7 Aug. 2008[a], https://doi.org/10.1029/2007jc004124. Accessed 15 Mar. 2023.

Jones, E. P., Anderson, L.G., Jutterström, S., and Swift, J. H. "Sources and Distribution of Fresh Water in the East Greenland Current." *Progress in Oceanography*, vol. 78, no. 1, July 2008[b], pp. 37–44., https://doi.org/10.1016/j.pocean.2007.06.003. Accessed 9 Dec. 2022.

Jones, E. P., Anderson, L.G., and Swift, J. H. "Distribution of Atlantic and Pacific Waters in the Upper Arctic Ocean: Implications for Circulation." *Geophysical Research Letters*, vol. 25,

no. 6, 15 Mar. 1998, pp. 765–768., https://doi.org/10.1029/98gl00464. Accessed 17 Sept. 2022.

Jones, E. P., Swift, J. H., Anderson, L. G., Lipizer, M., Civitarese, G., Falkner, K. K., Kattner, G., and McLaughlin, F. "Tracing Pacific Water in the North Atlantic Ocean." *Journal of Geophysical Research*, vol. 108, no. C4, 12 Apr. 2003, https://doi.org/10.1029/2001jc001141. Accessed 2 Nov. 2022.

Karl, D., Michaels, A., Bergman, B., Capone, D., Carpenter, E., Letelier, R., Lipschultz, F., Paerl, H., Sigman, D., and Stal, L. "Dinitrogen Fixation in the World's Oceans." *Biogeochemistry*, 2002, pp. 47–98., https://doi.org/10.1007/978-94-017-3405-9_2. Accessed 4 Mar. 2023.

Katsman, C. A., Spall, M. A., and Pickart, R. S. "Boundary Current Eddies and Their Role in the Restratification of the Labrador Sea*." *Journal of Physical Oceanography*, vol. 34, no. 9, 1 Sept. 2004, pp. 1967–1983., https://doi.org/10.1175/1520-0485(2004)034<1967:bceatr>2.0.co;2. Accessed 1 May 2023.

Key, R. 2022. Bottle data from cruise 06MT19970815, WHP netCDF version. Accessed from CCHDO https://cchdo.ucsd.edu/cruise/06MT19970815. Access date 2022-09-04.

Lalli, C. M. and Timothy R. Parsons. *Biological Oceanography: An Introduction*. Second ed., Butterworth-Heinemann, 1993.

Le Bras, I. A., Straneo, F., Holte, J., and Holliday, N. P., "Seasonality of Freshwater in the East Greenland Current System from 2014 to 2016." *Journal of Geophysical Research: Oceans*, vol. 123, no. 12, 2018, pp. 8828–8848., https://doi.org/10.1029/2018jc014511. Accessed 5 Sept. 2022.

Lherminier, P. 2022. Bottle and CTD data from cruise 06MM20060523, WHP netCDF version. Accessed from CCHDO https://cchdo.ucsd.edu/cruise/06MM20060523. Access date 2022-08-28.

Lherminier, P., Perez, F., Branellec, P., Mercier, H., Velo, A., Messias, M., Castrillejo, M., Reverdin, G., Fontela, M., Baurand, F. (2022). GO-SHIP A25 - OVIDE 2018 Cruise bottle and CTD data. SEANOE. https://doi.org/10.17882/87394

Lordan, R., Tsoupras, A., and Zabetakis, I. "Phospholipids of Animal and Marine Origin: Structure, Function, and Anti-Inflammatory Properties." *Molecules*, Nov. 2017, https://doi.org/10.20944/preprints201711.0038.v1. Accessed 11 Apr. 2023.

Luo, H., Castelao, R. M., Rennermalm, A. K., Tedesco, M. Bracco, A., Yager, P. L., and Mote, T. L. "Oceanic Transport of Surface Meltwater from the Southern Greenland Ice Sheet." *Nature Geoscience*, vol. 9, no. 7, July 2016, pp. 528–532., https://doi.org/10.1038/ngeo2708. Accessed 14 Feb. 2023.

Martiny, A. C., Pham, C. T., Primeau, F. W., Vrugt, J. A., Moore, J. K., Levin, S. A., and Lomas, M. W., "Strong Latitudinal Patterns in the Elemental Ratios of Marine Plankton and Organic Matter." *Nature Geoscience*, vol. 6, no. 4, Apr. 2013[a], pp. 279–283., https://doi.org/10.1038/ngeo1757. Accessed 7 Apr. 2023.

Martiny, A. C., Vrugt, J. A., Primeau, F. W., and Lomas, M. W., "Regional Variation in the Particulate Organic Carbon to Nitrogen Ratio in the Surface Ocean." *Global Biogeochemical Cycles*, vol. 27, no. 3, 18 Aug. 2013[b], pp. 723–731., https://doi.org/10.1002/gbc.20061. Accessed 7 Apr. 2023.

Meincke, J. 2022. Bottle data from cruise 06MT18_1, WHP netCDF version. Accessed from CCHDO https://cchdo.ucsd.edu/cruise/06MT18_1. Access date 2022-09-11.

Meire, L., Meire, P., Struyf, E., Krawczyk, D. W., Arendt, K. E., Yde, J. C., Juul Pedersen, T., Hopwood, M. J., Rysgaard, S., and Meysman, F. J. "High Export of Dissolved Silica from the Greenland Ice Sheet." *Geophysical Research Letters*, vol. 43, no. 17, 23 Aug. 2016, pp. 9173–9182., https://doi.org/10.1002/2016gl070191. Accessed 11 Dec. 2022.

Mercier, H. 2022. Bottle and CTD data from cruise 35TH20020610, WHP netCDF version. Accessed from CCHDO https://cchdo.ucsd.edu/cruise/35TH20020610. Access date 2022-08-28. CCHDO cruise DOI 10.1029/2006JC003716.

Mercier, H. 2022. Bottle and CTD data from cruise 35TH20080610, WHP netCDF version. Accessed from CCHDO https://cchdo.ucsd.edu/cruise/35TH20080610. Access date 2022-08-28.

Mercier, H., Lherminier, P., and Perez, F. (2022). The Greenland-Portugal Go-Ship A25 OVIDE CTDO2 hydrographic data. SEANOE. https://doi.org/10.17882/46448

Moore, C. M., Mills, M. M., Arrigo, K. R., Berman-Frank, I., Bopp, L., Boyd, P. W., Galbraith, E. D., Geider, R. J., Guieu, C., Jaccard, S. L., Jickells, T. D., La Roche, J., Lenton, T. M., Mahowald, N. M., Marañón, E., Marinov, I., Moore, J. K., Nakatsuka, T., Oschlies, A., Saito, M. A., Thingstad, T. F., Tsuda, A., and Ulloa, O. "Processes and Patterns of Oceanic Nutrient Limitation." *Nature Geoscience*, vol. 6, no. 9, Sept. 2013, pp. 701–710., https://doi.org/10.1038/ngeo1765. Accessed 10 Apr. 2023.

Pawlowicz, R., 2020. "M_Map: A mapping package for MATLAB", version 1.4m, *Matlab R2022b,* www.eoas.ubc.ca/~rich/map.html.

Paytan, Adina, and Karen McLaughlin. "The Oceanic Phosphorus Cycle." *ChemInform*, vol. 38, no. 20, 15 Jan. 2007, pp. 563–576., https://doi.org/10.1002/chin.200720268. Accessed 1 Nov. 2022.

Perez, F. 2022. Bottle and CTD data from cruise 29AH20160617, csv version. Access from CCHDO https://cchdo.ucsd.edu/cruise/29AH20160617. Access date 2022-08-28. CCHDO cruise DOI 10.13155/59190.

Perez, F., Treguer, P., Branellec, P., García-Ibáñez, M. I., Lherminier, P., & Sarthou, G. (2020). The 2014 Greenland-Portugal GEOVIDE bottle data (GO-SHIP A25 and GEOTRACES GA01). SEANOE. https://doi.org/10.17882/54653.

Pérez-Hernández, M. D., Pickart, R.S., Pavlov, V., Våge, K., Ingvaldsen, R., Sundfjord, A. Renner, A., Torres, D. and Erofeeva, S. "The Atlantic Water Boundary Current North of Svalbard in Late Summer." *Journal of Geophysical Research: Oceans*, vol. 122, no. 3, 2017, pp. 2269–2290., https://doi.org/10.1002/2016jc012486. Accessed 16 Jan. 2023.

Pickart, R. (2018). Conductivity-Temperature-Depth bottle data as part of the OSNAP (Overturning in the Subpolar North Atlantic Program), from 2016 on the R/V Neil Armstrong. Duke Digital Repository. https://doi.org/10.7924/r4m61gc19

Quay, Paul. "Impact of the Elemental Composition of Exported Organic Matter on the Observed Dissolved Nutrient and Trace Element Distributions in the Upper Layer of the Ocean." *Global Biogeochemical Cycles*, vol. 35, no. 10, 18 Sept. 2021, https://doi.org/10.1029/2020gb006902. Accessed 10 Apr. 2023.

Quigg, A., Finkel, Z. V., Irwin, A. J., Rosenthal, Y., Ho, T., Reinfelder, J. R., Schofield, O., Morel, F. M., and Falkowski, P. G. "The Evolutionary Inheritance of Elemental Stoichiometry in Marine Phytoplankton." *Nature*, vol. 425, no. 6955, 18 Sept. 2003, pp. 291–294., https://doi.org/10.1038/nature01953. Accessed 5 Apr. 2023.

Redfield, Alfred C. "The Biological Control of Chemical Factors in the Environment." *American Scientist*, vol. 46, Sept. 1958, pp. 205–221., https://ebme.marine.rutgers.edu/HistoryEarthSystems/HistEarthSystems_Fall2008/Week4b/Redfield_AmSci_1958.pdf. Accessed 10 Oct. 2022.

Rignot, E., Box, J. E., Burgess, E., and Hanna, E. "Mass Balance of the Greenland Ice Sheet from 1958 to 2007." *Geophysical Research Letters*, vol. 35, no. 20, 22 Oct. 2008, https://doi.org/10.1029/2008gl035417. Accessed 12 Feb. 2023.

Rios, A. 2022. Bottle and CTD data from cruise 29AH20120622, WHP netCDF version. Accessed from CCHDO https://cchdo.ucsd.edu/cruise/29AH20120622. Access date 2022-08-28.

Rudels, B., Björk, G., Nilsson, J., Winsor, P., Lake, I., and Nohr, C. "The Interaction between Waters from the Arctic Ocean and the Nordic Seas North of Fram Strait and along the East Greenland Current: Results from the Arctic Ocean-02 Oden Expedition." *Journal of Marine Systems*, vol. 55, no. 1-2, 2005, pp. 1–30., https://doi.org/10.1016/j.jmarsys.2004.06.008. Accessed 14 Feb. 2022.

Rudels, B., Korhonen, M., Schauer, U., Pisarev, S., Rabe, B., and Wisotzki, A. "Circulation and Transformation of Atlantic Water in the Eurasian Basin and the Contribution of the Fram Strait Inflow Branch to the Arctic Ocean Heat Budget." *Progress in Oceanography*, vol.

132, Mar. 2015, pp. 128–152., https://doi.org/10.1016/j.pocean.2014.04.003. Accessed 10 Jan. 2023.

Sabine, C. L., Feely, R. A., Gruber, N., Key, R. M., Lee, K., Bullister, J. L., Wanninkhof, R., Wong, C. S., Wallace, D. W. R., Tillbrook, B., Millero, F. J., Peng, T., Kozyr, A., Ono, T., and Rios, A. F. "The Oceanic Sink for Anthropogenic CO2." *Science*, vol. 305, no. 5682, 16 July 2004, pp. 367–371, https://www.pmel.noaa.gov/pubs/outstand/sabi2683/sabi2683.shtml.

Sanz-Luque, E., Chamizo-Ampudia, A., Llamas, A., Galvan, A., and Fernandez, E. "Understanding Nitrate Assimilation and Its Regulation in Microalgae." *Frontiers in Plant Science*, vol. 6, Oct. 2015, https://doi.org/10.3389/fpls.2015.00899. Accessed 4 Apr. 2023.

Sarafanov, A., Falina, A., Mercier, H., Sokov, A., Lherminier, P., Gourcuff, C., Gladyshev, S., Gaillard, F., and Daniault, N. "Mean Full-Depth Summer Circulation and Transports at the Northern Periphery of the Atlantic Ocean in the 2000s." *Journal of Geophysical Research: Oceans*, vol. 117, no. C1, 24 Jan. 2012, https://doi.org/10.1029/2011jc007572. Accessed 15 Apr. 2023.

Sarthou, G. and Lherminier, P. 2022. CTD data from cruise 35PK20140515, WHP netCDF version. Accessed from CCHDO https://cchdo.ucsd.edu/cruise/35PK20140515. Access date 2022-08-28.

Schott, F. 2022. Bottle data from cruise 06MT39_4, nc version. Accessed from CCHDO https://cchdo.ucsd.edu/cruise/06MT39_4. Access date 2022-09-11.

Steele, M., Morison, J., Ermold, W., Rigor, I., Ortmeyer, M., and Shimada, K. "Circulation of Summer Pacific Halocline Water in the Arctic Ocean." *Journal of Geophysical Research*, vol. 109, no. C2, Feb. 2004, https://doi.org/10.1029/2003jc002009. Accessed 15 Jan. 2023.

Sutherland, D. A., Pickart, R. S., Jones, E. P., Azetsu-Scott, K., Eert, A. J., and Ólafsson, J. "Freshwater Composition of the Waters off Southeast Greenland and Their Link to the Arctic Ocean." *Journal of Geophysical Research*, vol. 114, no. C5, 27 May 2009, https://doi.org/10.1029/2008jc004808. Accessed 2 Sept. 2022.

Sutherland, David A. and Robert S. Pickart. "The East Greenland Coastal Current: Structure, Variability, and Forcing." *Progress in Oceanography*, vol. 78, no. 1, 2008, pp. 58–77., https://doi.org/10.1016/j.pocean.2007.09.006. Accessed 24 Sept. 2022.

Teng, Y., Primeau, F. W., Moore, J. K., Lomas, M. W., and Martiny, A. C. "Global-Scale Variations of the Ratios of Carbon to Phosphorus in Exported Marine Organic Matter." *Nature Geoscience*, vol. 7, no. 12, Dec. 2014, pp. 895–898., https://doi.org/10.1038/ngeo2303. Accessed 10 Apr. 2023.

Tesdal, J., Ducklow, H. W., Goes, J. I., and Yashayaev, I. "Recent Nutrient Enrichment and High Biological Productivity in the Labrador Sea Is Tied to Enhanced Winter Convection." *Progress in Oceanography*, vol. 206, 2022, https://doi.org/10.1016/j.pocean.2022.102848. Accessed 4 Sept. 2022.

*The Gibbs Seawater (GSW) Oceanographic Toolbox of TEOS-10*, https://www.teos-10.org/pubs/gsw/html/gsw_contents.html.

Toggweiler, J. R. "Oceanography: An Ultimate Limiting Nutrient." *Nature*, vol. 400, no. 6744, 5 Aug. 1999, pp. 511–512., https://doi.org/10.1038/22892. Accessed 12 Nov. 2022.

Tréguer, Paul J., and Christina L. De La Rocha. "The World Ocean Silica Cycle." *Annual Review of Marine Science*, vol. 5, no. 1, Jan. 2013, pp. 477–501., https://doi.org/10.1146/annurev-marine-121211-172346. Accessed 2 Mar. 2023.

Tréguer, P., Nelson, D. M., Van Bennekom, A. J., DeMaster, D. J., Leynaert, A., and Quéguiner, B. "The Silica Balance in the World Ocean: A Reestimate." *Science*, vol. 268, no. 5209, 21 Apr. 1995, pp. 375–379., https://doi.org/10.1126/science.268.5209.375. Accessed 5 Mar. 2023.

Tuerena, R. E., Hopkins, J., Buchanan, P. J., Ganeshram, R. S., Norman, L., von Appen, W., Tagliabue, A., Doncila, A., Graeve, M., Ludwichowski, K. U., Dodd, P. A., de la Vega, C., Salter, I., and Manhaffey, C. "An Arctic Strait of Two Halves: The Changing Dynamics of Nutrient Uptake and Limitation across the Fram Strait." *Global Biogeochemical Cycles*, vol. 35, no. 9, 9 Aug. 2021, https://doi.org/10.1029/2021gb006961. Accessed 20 Apr. 2023.

Tyrrell, Toby. "The Relative Influences of Nitrogen and Phosphorus on Oceanic Primary Production." *Nature*, vol. 400, no. 6744, 5 Aug. 1999, pp. 525–531., https://doi.org/10.1038/22941. Accessed 1 Nov. 2022.

Våge, K., Pickart, R. S., Sarafanov, A., Knutsen, Ø., Mercier, H., Lherminier, P., van Aken, H., Meincke, J., Quadfasel, D., & Bacon, S. "The Irminger Gyre: Circulation, Convection, and Interannual Variability." *Deep Sea Research Part I: Oceanographic Research Papers*, vol. 58, no. 5, 2011, pp. 590–614., https://doi.org/10.1016/j.dsr.2011.03.001. Accessed 30 Nov. 2022.

Vernet, M., Ellingsen, I., Marchese, C., Bélanger, S., Cape, M., Slagstad, D., and Matrai, P. A. "Spatial Variability in Rates of Net Primary Production (NPP) and Onset of the Spring Bloom in Greenland Shelf Waters." *Progress in Oceanography*, vol. 198, Nov. 2021, p. 102655., https://doi.org/10.1016/j.pocean.2021.102655. Accessed 14 Sept. 2022.

Veth, C. 2022. Bottle and CTD data from cruise 64PE20050907, WHP netCDF version. Accessed from CCHDO https://cchdo.ucsd.edu/cruise/64PE20050907. Access date 2022 09-07.

Villareal, T. A., Pilskaln, C., Brzezinski, M. Lipschultz, F., Dennett, M., and Gardner, G. B. "Upward Transport of Oceanic Nitrate by Migrating Diatom Mats." *Nature*, vol. 397, no. 6718, 4 Feb. 1999, pp. 423–425., https://doi.org/10.1038/17103. Accessed 7 Apr. 2023.

Voss, M., Bange, H. W., Dippner, J. W., Middelburg, J. J., Montoya, J. P., and Ward, B. "The Marine Nitrogen Cycle: Recent Discoveries, Uncertainties and the Potential Relevance of Climate Change." *Philosophical Transactions of the Royal Society B: Biological Sciences*, vol. 368, no. 1621, 5 July 2013, https://doi.org/10.1098/rstb.2013.0121. Accessed 6 Nov. 2022.

Warsi, Omar M., and Daniel E. Dykhuizen. "Evolutionary Implications of Liebig's Law of the Minimum: Selection under Low Concentrations of Two Nonsubstitutable Nutrients." *Ecology and Evolution*, vol. 7, no. 14, July 2017, pp. 5296–5309., https://doi.org/10.1002/ece3.3096. Accessed 11 Apr. 2023.

Yahia, E., Carrillo-López, A., Malda Barrera, G., Suzán-Azpiri, H., and Queijeiro Bolaños, M., editors. "Chapter 3: Photosynthesis." *Postharvest Physiology and Biochemistry of Fruits and Vegetables*, Woodhead Publishing, Duxford, 2019, pp. 47–72.

Yamamoto-Kawai, M., Carmack, E., and McLaughlin, F. "Nitrogen Balance and Arctic Throughflow." *Nature*, vol. 443, no. 7107, 7 Sept. 2006, pp. 43–43., https://doi.org/10.1038/443043a. Accessed 20 Feb. 2023.

Zehr, Jonathan P. and Ward, B. B. "Nitrogen Cycling in the Ocean: New Perspectives on Processes and Paradigms." *Applied and Environmental Microbiology*, vol. 68, no. 3, 1 Mar. 2002, pp. 1015–1024., https://doi.org/10.1128/aem.68.3.1015-1024.2002. Accessed 9 Dec. 2022.

*Contains data supplied by the Natural Environment Research Council. This study uses data from data Institute of Oceanographic Sciences, Deacon Laboratory, provided by the British Oceanographic Data Centre and funded by the World Climate Research Program, WCRP-11 and 12, WMO/ICSU 1988.